Cell Reports

Article

Activation of GPR44 decreases severity of myeloid leukemia via specific targeting of leukemia initiating stem cells

Graphical abstract

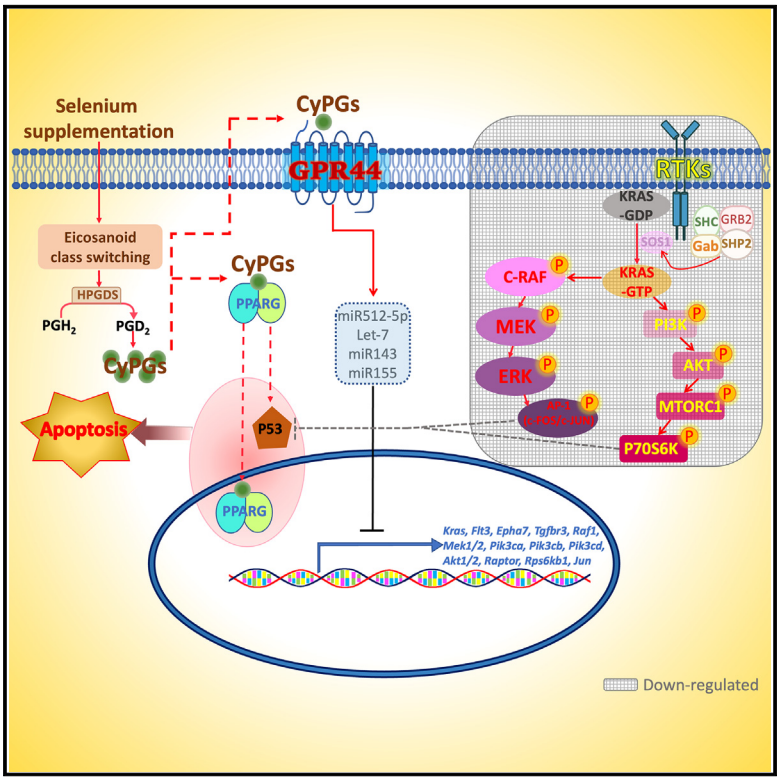

Highlights

- Exogenous and dietary selenium supplementation-induced endogenous CyPGs target LICs
- CyPG-dependent activation of GPR44 leads to apoptosis of LICs, sparing normal HSCs
- GPR44 deletion in LICs enhances RTK-activated KRAS-MAPK and -PI3K/AKT/mTORC axes
- Loss of GPR44 increases aggressiveness of AML

Authors

Fenghua Qian, Shaneice K. Nettleford, Jiayan Zhou, ..., David F. Claxton, Robert F. Paulson, K. Sandeep Prabhu

Correspondence

rfp5@psu.edu (R.F.P.), ksp4@psu.edu (K.S.P.)

In brief

Qian et al. describe an important mechanism by which dietary selenium enhances H-PGDS expression that favors production of cyclopentenone prostaglandin (CyPG) production. In addition to activating PPARγ, CyPGs activate GPR44 to suppress RTK-activated KRAS-mediated MAPK and PI3K/AKT/mTORC1 pathways, leading to the P53-mediated apoptosis in AML.

Qian et al., 2023, Cell Reports *42*, 112794
July 25, 2023 © 2023 The Author(s).
https://doi.org/10.1016/j.celrep.2023.112794

CellPress

Cell Reports

CellPress
OPEN ACCESS

Article

Activation of GPR44 decreases severity of myeloid leukemia via specific targeting of leukemia initiating stem cells

Fenghua Qian,[1] Shaneice K. Nettleford,[1] Jiayan Zhou,[1] Brooke E. Arner,[1] Molly A. Hall,[1] Arati Sharma,[2] Charyguly Annageldiyev,[2] Randy M. Rossi,[3] Diwakar B. Tukaramrao,[2] Deborpita Sarkar,[1] Shailaja Hegde,[4] Ujjawal H. Gandhi,[5] Emily R. Finch,[6] Laura Goodfield,[7] Michael D. Quickel,[1] David F. Claxton,[2] Robert F. Paulson,[1,*] and K. Sandeep Prabhu[1,8,*]

[1]Department of Veterinary and Biomedical Sciences, The Pennsylvania State University, University Park, PA 16802, USA
[2]Department of Medicine, Division of Hematology and Oncology, Penn State Cancer Institute, The Pennsylvania State University College of Medicine, Hershey, PA 17033, USA
[3]Transgenic Core Facility, Huck Institute of the Life Sciences, The Pennsylvania State University, University Park, PA 16802, USA
[4]Hoxworth Blood Center, Division of Experimental Hematology and Cancer Biology, Cincinnati Children's Hospital Medical Center, University of Cincinnati College of Medicine, Cincinnati, OH 45267, USA
[5]Department of Hematology and Oncology, University of North Carolina Health, Cary, NC 27518, USA
[6]Department of Biostatistics, St. Jude Children's Research Hospital, Memphis, TN 38105, USA
[7]Immunooncology Division, Bicycle Therapeutics, Boston, MA 02140, USA
[8]Lead contact
*Correspondence: rfp5@psu.edu (R.F.P.), ksp4@psu.edu (K.S.P.)
https://doi.org/10.1016/j.celrep.2023.112794

SUMMARY

Relapse of acute myeloid leukemia (AML) remains a significant concern due to persistent leukemia-initiating stem cells (LICs) that are typically not targeted by most existing therapies. Using a murine AML model, human AML cell lines, and patient samples, we show that AML LICs are sensitive to endogenous and exogenous cyclopentenone prostaglandin-J (CyPG), Δ^{12}-PGJ$_2$, and 15d-PGJ$_2$, which are increased upon dietary selenium supplementation via the cyclooxygenase-hematopoietic PGD synthase pathway. CyPGs are endogenous ligands for peroxisome proliferator-activated receptor gamma and GPR44 (CRTH2; PTGDR2). Deletion of GPR44 in a mouse model of AML exacerbated the disease suggesting that GPR44 activation mediates selenium-mediated apoptosis of LICs. Transcriptomic analysis of GPR44$^{-/-}$ LICs indicated that GPR44 activation by CyPGs suppressed KRAS-mediated MAPK and PI3K/AKT/mTOR signaling pathways, to enhance apoptosis. Our studies show the role of GPR44, providing mechanistic underpinnings of the chemopreventive and chemotherapeutic properties of selenium and CyPGs in AML.

INTRODUCTION

Acute myeloid leukemia (AML) represents a malignancy characterized by infiltration of abnormally proliferating hematopoietic progenitor and stem cells (HPSCs) in the bone marrow, blood, and other tissues.[1] Cytogenetic and molecular heterogeneity of AML has led to refractoriness and relapse.[2,3] A key impediment in the treatment is the minimal residual disease (MRD),[4,5] characterized by the presence of leukemia-initiating stem cells (LICs) that are, in part, crucial for the relapse of disease.[6] These cells resemble normal HPSCs in terms of self-renewal, proliferation, and differentiation. Therefore, alternative therapies that target LICs open new avenues to treat AML and other malignancies as the cancer stem cell component continues to be better defined.[7]

Early studies showed that selenium (Se) cystine effectively treated AML and chronic myeloid leukemia (CML) patients, resulting in improved leukocytosis and decreased spleen size.[8] Since then, *in vitro* and *in vivo* studies have confirmed the anti-leukemic effect of trace element Se.[9–11] Previously, we reported that Se at supraphysiological levels affected the viability of LICs in CML[12] via skewing the arachidonic acid metabolism toward the anti-inflammatory cyclopentenone prostaglandins (CyPGs), while decreasing the pro-inflammatory PGE$_2$ and thromboxane B$_2$.[13,14] Previous studies reported that CyPGs enhanced the ATM-p53 axis via the peroxisome proliferator activated receptor gamma (PPARγ) activation in CML-LICs.[12,15] Recently we showed that CyPGs induced by exogenous interleukin-4 benefit AML via activating PPARγ.[16] Interestingly, apart from PPARγ, CyPGs also bind with much greater affinity to GPR44 (also called CRTH2 or DP2), a G protein coupled receptor (GPCR).[17,18] GPR44 is expressed on multiple cell types but mainly on Th2 effector cells[19] and most of the literature on GPR44 pertains to its role in autoimmune diseases and type 2 immunity[19,20] with a significant lack of research into its role in hematologic malignancies.

This is an open access article under the CC BY-NC-ND license (http://creativecommons.org/licenses/by-nc-nd/4.0/).

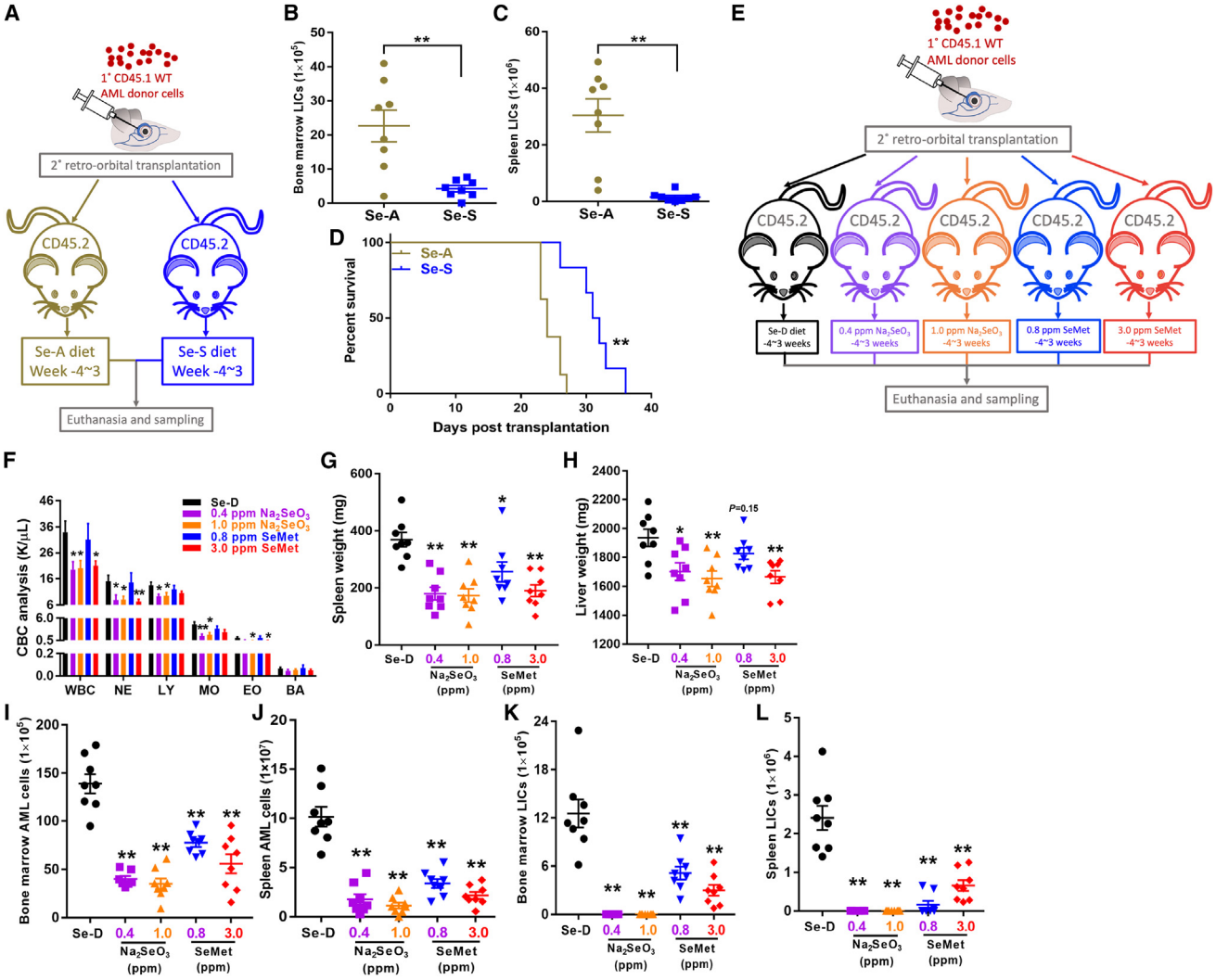

Figure 1. Se supplementation improves the outcome of AML

(A) CD45.2-recipient mice were maintained on diets (Se-A or Se-S) for 4 weeks before retro-orbital transplantation with 1° CD45.1 WT AML donor cells; 3 weeks later, mice were euthanized, and blood, bone marrow, and spleen were sampled (n = 8 in each group).

(B and C) Counts of LICs ($CD45.1^+Lin^-Sca\text{-}1^-c\text{-}Kit^+$, see also Figure S1J) in the bone marrow (B) and spleen (C) of AML mice in (A).

(D) Survival curve of recipient mice on Se-A (n = 8) or Se-S (n = 6) diet secondarily transplanted with WT AML donor cells.

(E) CD45.2-recipient mice were maintained on diets (Se-D, 0.4 or 1.0 ppm Na_2SeO_3, and 0.8 or 3.0 ppm SeMet) for 4 weeks before retro-orbital transplantation with 1° CD45.1 WT AML donor cells; 3 weeks later, mice were euthanized, and blood, serum, bone marrow, and spleen were sampled (n = 8 in each group).

(F) CBC (K/μL peripheral blood) analysis of AML mice at the endpoint in (E).

(G and H) Spleen (G) and liver (H) weights (mg) of AML mice in (E).

(I and J) Counts of AML cells ($CD45.1^+$) in the Lin^- population in the bone marrow (I) and spleen (J) of AML mice in (E).

(K and L) Counts of LICs ($CD45.1^+Lin^-Sca\text{-}1^-c\text{-}Kit^+$, see also Figure S1J) in the bone marrow (K) and spleen (L) of AML mice in (E).

Data shown are mean ± SEM per group; each dot represents a mouse; *$p < 0.05$, **$p < 0.01$.

Here, we show that activation of GPR44 mediates the anti-leukemic effect of endogenous CyPGs generated upon Se supplementation in LICs in a murine AML model and patient-derived AML cells. Furthermore, activation of GPR44 by CyPGs suppressed KRAS-mediated MAPK and PI3K/AKT/mTOR signaling pathways, enhancing apoptosis of AML LICs. These studies highlight an important therapeutic role for GPR44 in leukemia and provide mechanistic underpinnings for the chemopreventive properties of Se and CyPGs in AML.

RESULTS

Se supplementation improves the outcome of AML

To examine the effect of Se supplementation at supraphysiological levels on the outcome of AML, CD45.2 mice maintained on an AIN-76 diet containing Se (sodium selenite, Na_2SeO_3) at either 0.08 ppm (Se-A, Se-adequate) or 0.4 ppm (Se-S, Se-supplemented) were transplanted with $CD45.1^+$ primary (1°) WT AML donor cells (Figure 1A) to generate secondary AML mice as

CellPress
OPEN ACCESS

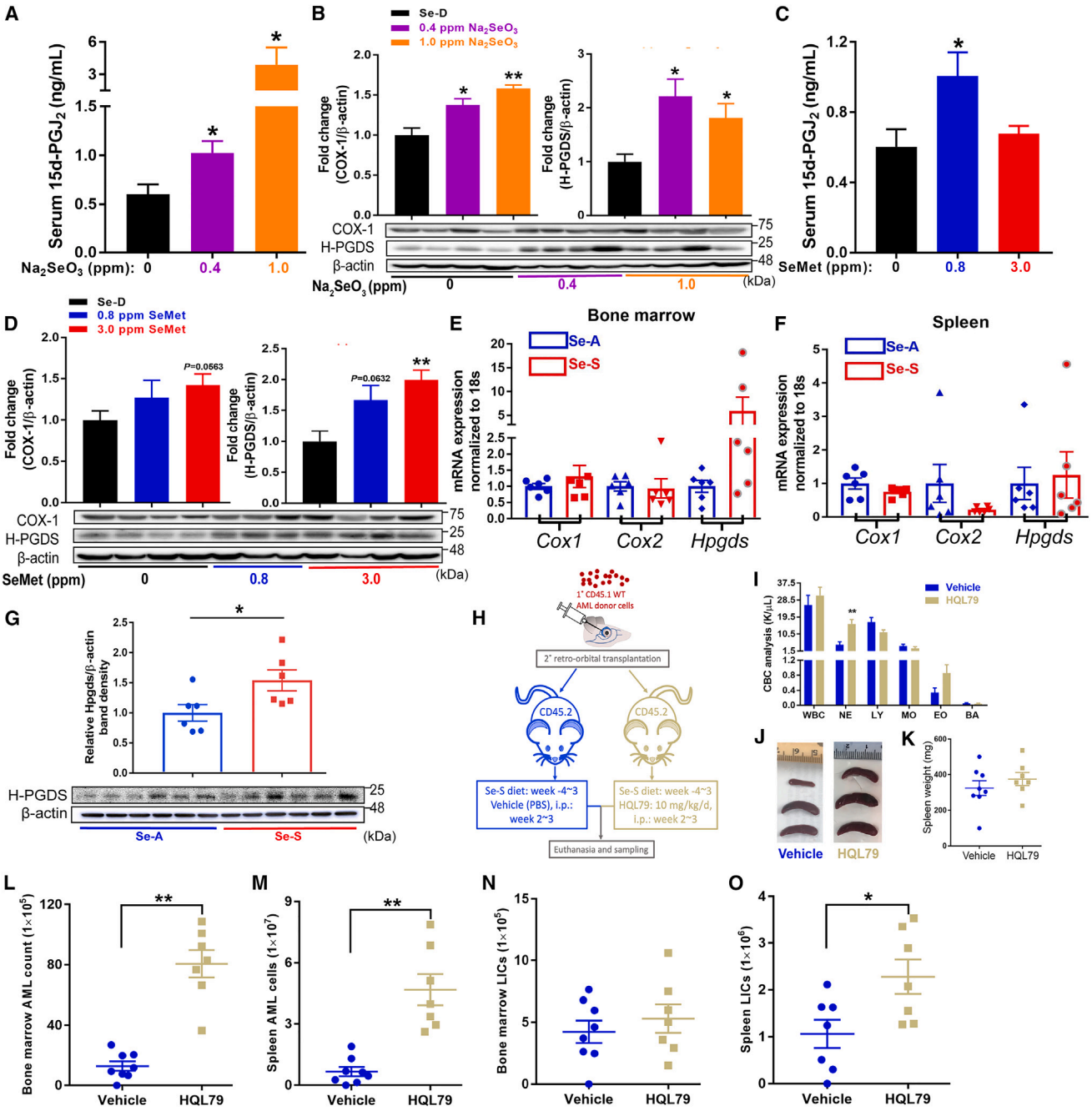

Figure 2. Se supplement induces endogenous production of CyPGs in AML

(A) Serum level of 15d-PGJ$_2$ of AML mice on Se-D, 0.4 ppm Na_2SeO_3, and 1.0 ppm Na_2SeO_3 diets measured by ELISA (n = 7–8 in each group).

(B) Western blot showing expression of COX-1 and H-PGDS in cells isolated from spleens of AML mice on Se-D, 0.4 ppm Na_2SeO_3, and 1.0 ppm Na_2SeO_3 diets.

(C) Serum level of 15d-PGJ$_2$ of AML mice on Se-D, 0.8 ppm SeMet, and 3.0 ppm SeMet diets measured by ELISA (n = 7–8 in each group).

(D) Western blot showing expression of COX-1 and H-PGDS in cells isolated from spleens of AML mice on Se-D, 0.8 ppm SeMet, and 3.0 ppm SeMet diets.

(B and D) Densitometry was done by normalizing to Se-D group and relative to β-actin (n = 3–4 in each group).

(E and F) Expression of genes (*Cox1*, *Cox2*, and *Hpgds*) assessed by qPCR analysis in the bone marrow (E) and spleen (F) of AML mice on Se-A and Se-S diets. Data were normalized to Se-A group and *18S* rRNA expression (n = 5–6 in each group).

(G) Western blot showing expression of H-PGDS in cells isolated from bone marrow of AML mice on Se-A and Se-S diets. Densitometry was done by normalizing to Se-A group and relative to β-actin (n = 6 in each group).

(H) CD45.2-recipient mice were maintained on Se-S diet for 4 weeks before retro-orbital transplantation with 1° CD45.1 WT AML donor cells; 1 week later, HQL79 (10 mg/kg) or PBS (vehicle control) was administered i.p. daily for 2 weeks. Mice were euthanized after treatment, and blood, bone marrow, and spleen were sampled (n = 6–8 in each group).

(legend continued on next page)

described in Figures S1A–S1D. Mice maintained on the Se-S diet showed decreased leukocytosis (Figure S1E) as well as lower average spleen weight than their Se-A counterparts at the endpoint (Figure S1F and S1G). Se-S mice also showed significant reduction in tumor burden in the bone marrow (Figure S1H) and spleen (Figure S1I), indicated by CD45.1$^+$ cells in the Lin$^-$ population compared with their Se-A counterparts. WT LICs, identified as CD45.1$^+$Lin$^-$Sca-1$^-$c-Kit$^+$ cells (Figure S1J), were reduced in the Se-S group (Figures 1B and 1C). Analysis of recipient bone marrow cells in the form of Lin$^-$ population (CD45.1$^-$) (Figure S1K) and hematopoietic stem cells (HSCs) (CD45.1$^-$Lin$^-$Sca-1$^+$c-Kit$^+$) (Figures S1J and S1L) indicated that normal HSCs were unaffected by Se treatment. Importantly, Se supplementation contributed to a significantly prolonged survival of AML mice (Figure 1D).

We next compared the impact of different forms of dietary Se on the disease, particularly in targeting LICs in the AML mice. CD45.2-recipient mice maintained on Se-deficient (Se-D) diet (with no detectable levels of Se < 0.01 ppm) or other diets supplemented with 0.4 or 1.0 ppm of Na_2SeO_3 (inorganic), or 0.8 or 3.0 ppm of selenomethionine (SeMet; organic) prepared using the Se-D diet. These mice were transplanted with CD45.1$^+$ WT AML donor cells and euthanized at 3 weeks post transplantation (Figure 1E). Compared with the Se-D diet, all Se-enriched groups except 0.8 ppm SeMet had significantly improved leukocytosis with an overall reduction of leukocytes (Figure 1F). Mice exhibited decreased splenomegaly (Figures 1G and S1M) and hepatomegaly (Figures 1H and S1N) upon supplementation with Na_2SeO_3 or SeMet. AML cells in the Lin$^-$ population and LICs were greatly reduced in the bone marrow and spleen upon Se supplementation with Na_2SeO_3 or SeMet (Figures 1I–1L). *In vitro* Na_2SeO_3 also exerted an inhibitory effect on the viability of MOLM13 cells, an immortalized human cell line expressing MLL-AF9 fusion gene as in our murine AML model (Figure S1O).[21] Between Na_2SeO_3 and SeMet diet groups, we found that 0.4 ppm Na_2SeO_3 was sufficient, while 3 ppm of SeMet was required to achieve the optimal anti-leukemic effect, indicating a preventive advantage of Na_2SeO_3 over SeMet in AML.

Se supplementation induces endogenous production of CyPGs in AML

Analysis of serum 15d-PGJ$_2$ of AML mice indicated a Se dose-dependent increase in 15d-PGJ$_2$ in Na_2SeO_3-fed mice compared with those on the Se-D diet (Figure 2A), which corroborated well with the enhanced expression of upstream enzymes, cyclooxygenase-1 (COX-1) and hematopoietic PGD synthase (H-PGDS) (Figure 2B). A significant increase of serum 15d-PGJ$_2$ was only observed in 0.8 ppm SeMet-fed mice, but not in the 3.0 ppm SeMet group compared with the Se-D group (Figure 2C). While COX-1 expression showed an increased trend with SeMet, H-PGDS was only significantly increased in the 3.0 ppm SeMet group (Figure 2D). Since Na_2SeO_3 diets gave us more consistent results, we focused on this form of dietary Se for the remainder of this work. Analysis of the bone marrow and spleen from AML mice fed on commercially available Se-A or Se-S diets (Se added as Na_2SeO_3) showed a Se-dependent increase in the expression of H-PGDS and CyPGs in the Se-S group (Figures 2E–2G).

To further examine the underlying role of H-PGDS, we treated Se-S AML mice with HQL79, a potent inhibitor of H-PGDS,[22] to block the endogenous production of CyPGs (Figure 2H), as described previously.[23] Although we observed a modest effect on leukocytosis (Figure 2I) and splenomegaly (Figures 2J and 2K), increased tumor burden was seen upon HQL79 treatment in the bone marrow and spleen of Se-S mice (Figures 2L and 2M). LICs were increased upon HQL79 treatment in the spleen of Se-S mice, although not significant in the bone marrow (Figures 2N and 2O). Together, these results indicate that Se supplementation alleviates AML via enhanced endogenous CyPGs by increasing H-PGDS expression.

GPR44 activation decreases the severity of leukemias

We next examined if exogenous CyPGs could treat AML in Se-A mice. Mice on Se-A diet transplanted with 1° WT(CD45.1$^+$) AML donor cells were treated with CyPGs (DK-PGD$_2$, 15d-PGJ$_2$, Δ^{12}-PGJ$_2$, and Δ^{12}-PGJ$_3$ at 0.2 mg/kg/day, i.p.) for 2 weeks. Δ^{12}-PGJ$_3$ and Δ^{12}-PGJ$_2$ are derived from the COX/H-PGDS pathway of metabolism of eicosapentaenoic acid and arachidonic acid metabolism, respectively. While 15d-PGJ$_2$, Δ^{12}-PGJ$_2$, and Δ^{12}-PGJ$_3$ can modulate the activity of PPARγ and other proteins, including GPR44, DK-PGD$_2$ is a ligand that specifically activates GPR44.[24–27] CyPG-treated mice showed reduced CBC and resolved splenomegaly (Figures 3A–3D). Infiltration of total Lin$^-$ AML cells was significantly reduced in the bone marrow and spleen (Figures S2A and S2B) of CyPG-treated Se-A AML mice that corroborated well with reduced number of LICs (Figures S1J, 3E, and 3F). Importantly, *in vivo* treatment of these exogenous CyPGs did not affect the proliferation of normal HSCs in the bone marrow (Figures S1J and S2C). Sorted WT AML-LICs treated *in vitro* with these bioactive lipids showed decreased viability (Figures S2D and S2E). The colony-forming capacity of AML cells was also affected, as seen by the 25%∼50% decrease in AML CFUs by DK-PGD$_2$, 15d-PGJ$_2$, Δ^{12}-PGJ$_2$, and Δ^{12}-PGJ$_3$ (Figures S2F–S2H). All the compounds except DK-PGD$_2$ induced cell death of MOLM13 cells with IC$_{50}$ of 2.28, 1.71, and 5.5 μM for Δ^{12}-PGJ$_2$, Δ^{12}-PGJ$_3$, and 15d-PGJ$_2$, respectively (Figure S2I). Of note, Δ^{12}-PGJ$_3$ exhibited a time-dependent inhibition of MOLM13 cell viability at 500 nM, which is 3-fold lower than its IC$_{50}$ (Figure S2J). GPR44 expression was detected at the transcript and protein levels in

(I) CBC (K/μL peripheral blood) analysis of Se-S AML mice at the endpoint in (H).
(J) Representative image of spleens isolated from Se-S AML mice in (H).
(K) Spleen weights (mg) of Se-S AML mice in (H).
(L and M) Counts of AML cells (CD45.1$^+$) in the Lin$^-$ population in the bone marrow (L) and spleen (M) of Se-S AML mice treated with PBS or HQL79 (n = 7–8 in each group).
(N and O) Counts of LICs (CD45.1$^+$Lin$^-$Sca-1$^-$c-Kit$^+$, see also Figure S1J) in the bone marrow (N) and spleen (O) of AML mice in (H).
Data shown are mean ± SEM per group; each dot represents a mouse; *p < 0.05, **p < 0.01.

CellPress
OPEN ACCESS

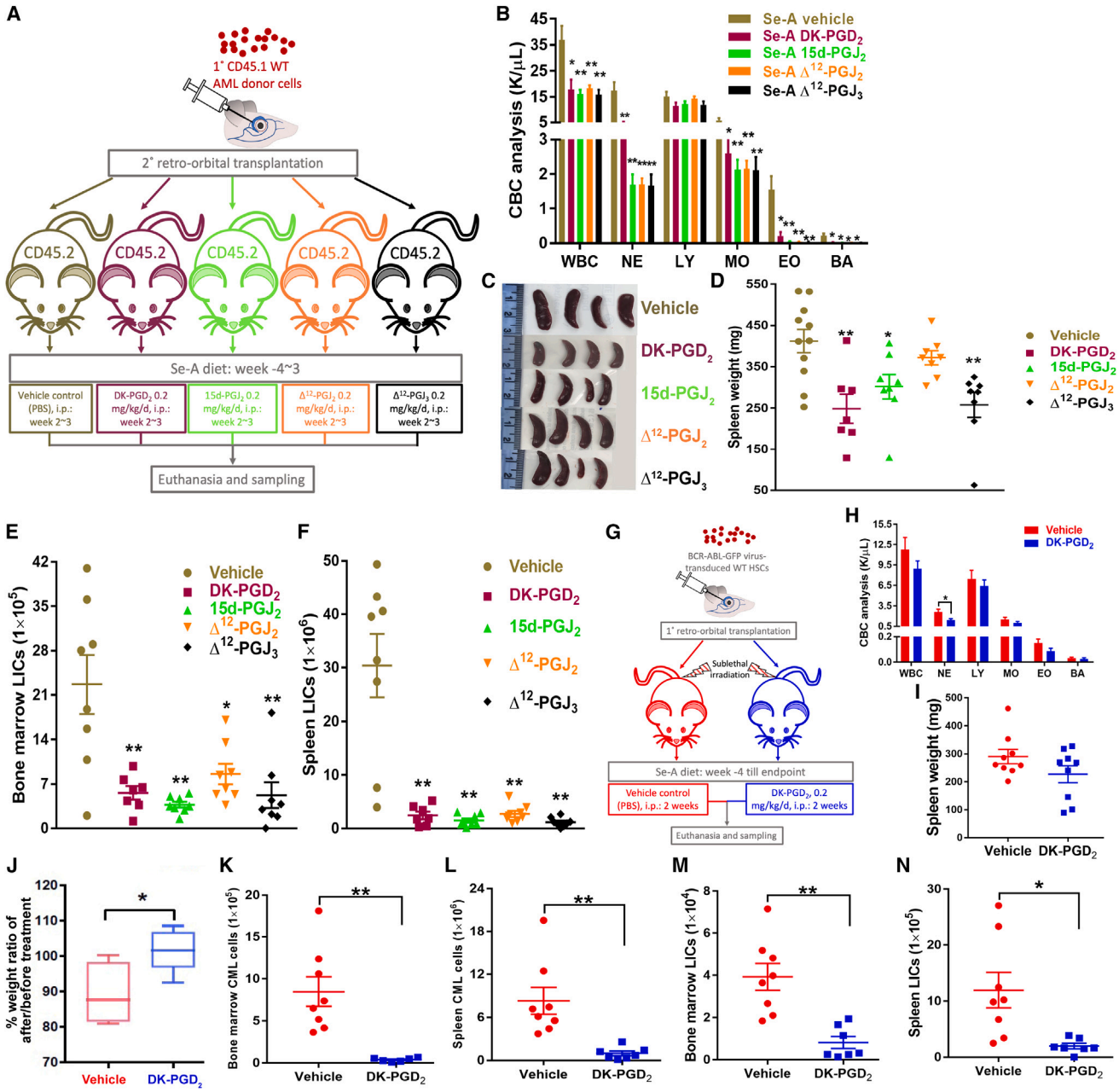

Figure 3. GPR44 activation decreases the severity of leukemia

(A) CD45.2-recipient mice were maintained on Se-A diet for 4 weeks before retro-orbital transplantation with 1° CD45.1 WT AML donor cells; at 1 week post transplantation, mice were treated i.p. daily with PBS or 0.2 mg/kg CyPGs (DK-PGD$_2$, 15d-PGJ$_2$, Δ^{12}-PGJ$_2$, and Δ^{12}-PGJ$_3$) for 2 weeks and euthanized after treatment; blood, bone marrow, and spleen were sampled (n = 7–8 in each group).

(B) CBC analysis of AML mice at the endpoint in (A).

(C) Representative image of spleens isolated from AML mice in (A).

(D) Spleen weights (mg) of AML mice in (A).

(E and F) Counts of LICs (CD45.1$^+$Lin$^-$Sca-1$^-$c-Kit$^+$, see also Figure S1J) in the bone marrow (E) and spleen (F) of AML mice in (A).

(G) 1°-recipient mice were maintained on Se-A diet for 4 weeks before sublethal irradiation (4.75 Gys) and retro-orbital transplantation with GFP BCR-ABL-transduced HSCs; DK-PGD$_2$ (0.2 mg/kg) or PBS control was given daily i.p. starting when peripheral blood WBC is over 5 K/μL for 2 weeks post transplantation. Mice were euthanized after treatment and blood, bone marrow, and spleen were sampled (n = 7–9 in each group).

(H) CBC analysis of CML mice in (G).

(I) Spleen weights (mg) of CML mice in (G).

(legend continued on next page)

MOLM13 cells, but the plasma membrane form of GPR44 was not as abundant as in the total cell extracts (Figures S2K and S2L). Further studies indicated that GPR44 was mainly intracellular rather than cell membrane localized, as seen by staining of permeabilized and unpermeabilized MOLM13 cells (Figure S2M), emphasizing the importance of cell membrane localization of GPR44 in response to CyPGs in AML.

To verify the clinical relevance, patient-derived AML cells were treated with DK-PGD$_2$ or 15d-PGJ$_2$. Surprisingly, 9 out of the 12 AML patient samples were responsive to DK-PGD$_2$ with enhanced apoptosis (Figure S2N), while three patient samples were refractory to this treatment (Figure S2O). Interestingly, patient samples sensitive to DK-PGD$_2$ treatment showed higher expression of GPR44 with over 4-fold increase than the refractory samples, further highlighting the crucial role of GPR44 in AML (Figure S2P). A similar phenomenon was seen in 15d-PGJ$_2$ treatment (Figures S2Q–S2S). Use of a GPR44-selective antagonist CAY10471 reversed the pro-apoptotic effect of Δ^{12}-PGJ$_3$ in patient-derived AML blasts (Figure S2T), confirming the GPR44-mediated anti-leukemic effect of CyPGs in AML. Furthermore, the direct interaction between human GPR44 and CyPGs evaluated in an *in vitro* binding assay indicated high binding affinity of human GPR44 by Δ^{12}-PGJ$_2$ and Δ^{12}-PGJ$_3$ with K_i values of 41.4 and 23.1 nM, respectively (Figure S2U).

The role of GPR44 was also verified in the previously reported murine model of CML with dietary Se (Figures S3A–S3D),[12] where recipient mice on Se-A diet were treated with DK-PGD$_2$ (injected i.p. daily) for 2 weeks. The treatment was initiated when peripheral white blood cells reached 5 K/μL (Figure 3G) and LICs were examined as described in Figure S3D. Compared with the control group, CML mice treated with DK-PGD$_2$ showed an improvement in the form of reduced neutrophils, decreased trend in splenomegaly, and enhanced weight gain (Figures 3H–3J). Tumor burden was also decreased by DK-PGD$_2$ in the bone marrow and spleen of CML mice (Figures 3K and 3L) along with a selective ablation of LICs (Figures 3M and 3N). Furthermore, DK-PGD$_2$ treatment significantly attenuated the viability of a human CML cell line, K562 cells, in a time-dependent manner (Figure S3E). These studies highlight the role of GPR44 as a new target in the treatment of both CML and AML. Interestingly, we observed a significant reduction in serum 15d-PGJ$_2$ in AML mice compared with healthy counterparts (Figure S3F), suggesting the need to increase endogenous CyPGs or use exogenous CyPGs at pharmacological doses to effectively treat myeloid leukemias.

Lack of GPR44 in AML cells results in aggressive disease

Gpr44$^{-/-}$ AML was developed using mice derived from Gpr44$^{-/-}$ embryonic stem cells obtained from the KOMP repository (Figures S1A, S4A, and S4B). The absence of GPR44 expression was confirmed by western immunoblotting analysis of purified 1° Gpr44$^{-/-}$ AML cells (Figure 4A). WT recipients on a Se-S diet transplanted with Gpr44$^{-/-}$ AML cells had significantly greater leukocytosis (Figures 4B and 4C) and increased splenomegaly (Figures S4C and S4D). A greater than 2-fold increase in total Lin$^-$ AML cells and LICs in bone marrow and spleen was seen in Gpr44$^{-/-}$ AML cell-transplanted mice compared with their WT AML counterparts (Figures 4D–4G and S4E). Gpr44$^{-/-}$ AML cell-transplanted mice also presented with hyperglycemia and marked impairment of liver function characterized by elevated AST and LDH (Table S1). This response was consistent with an intrinsic effect of the Gpr44 mutation. Transplanting Gpr44$^{-/-}$ and WT AML cells at 50:50 ratio resulted in disease that was intermediate of that observed with 100% WT AML cells or Gpr44$^{-/-}$ AML cells (Figures 4H and 4I). Deletion of GPR44 led to a ~10-fold increase in colony-forming capacity of 1° AML cells (Figures 4J and 4K). Analysis of the ONCOMINE database suggested increased expression of GPR44 in acute lymphoid leukemia, chronic lymphoid leukemia, and CML, as well as AML (Figure 4L), specifically in FAB subtypes M2, M3, and M6 (Figure 4M). AML patients with higher GPR44 expression showed a slightly better survival (Figure S4F), suggesting that high GPR44 expression could be a target for CyPG treatment rather than a prognostic factor.

Manipulating PPARγ activity affects the progression of Gpr44$^{-/-}$ AML

Here, we examined the potential crosstalk between PPARγ and GPR44, two receptors with overlapping ligand preferences albeit at different affinities. Se-S mice transplanted with Gpr44$^{-/-}$ AML cells were treated with PPARγ-selective antagonist, GW9662 (Figure S5A) and exhibited significantly higher CBC than their vehicle-treated counterparts along with increased splenomegaly (Figures S5A–S5C), which is in agreement with the increased total Lin$^-$ AML cells and LICs (Figures S5D and S5E) detected in the spleen of GW9662-treated mice. However, only a slight increase in leukemic burden was found in the bone marrow (Figures S5F and S5G). This discrepancy could be due to the differential expression of PPARγ in the bone marrow and spleen of AML mice (Figure S5H), wherein higher levels of PPARγ expression in the bone marrow might need a higher dose of GW9662 for inhibition. In contrast, Gpr44$^{-/-}$ AML Se-S mice treated with rosiglitazone, a PPARγ agonist, showed decreased leukocytosis and splenomegaly (Figures S5I–S5K). Rosiglitazone treatment only decreased LICs in the spleen but barely affected Lin$^-$ leukemic cells in the bone marrow and spleen and LICs in the bone marrow of AML mice (Figures S5L–S5O). Overall, these data indicate that AML cells lacking GPR44 expression can still be partially targeted by Se or CyPGs via PPARγ signaling, leading to cell death possibly via P53 activation, but activation of GPR44 leads to a more robust response to ablate AML LICs.

Lack of GPR44 activates KRAS-MAPK signaling in AML cells

Sorted WT and Gpr44$^{-/-}$ AML LICs were subjected to RNA sequencing analysis followed by IPA and GSEA (Figure 5A).

(J) Weight gain of Se-A CML mice treated with or without DK-PGD$_2$ was expressed as the ratio of after and before treatment (n = 4 in each group).
(K and L) Counts of CML cells (GFP$^+$) in the Lin$^-$ population in the bone marrow (K) and spleen (L) of CML mice in (G).
(M and N) Counts of LICs (GFP$^+$Lin$^-$Sca-1$^+$c-Kit$^+$, see also Figure S3D) in the bone marrow (M) and spleen (N) of CML mice in (G).
Data shown are mean ± SEM per group; each dot represents a mouse; *$p < 0.05$, **$p < 0.01$.

CellPress
OPEN ACCESS

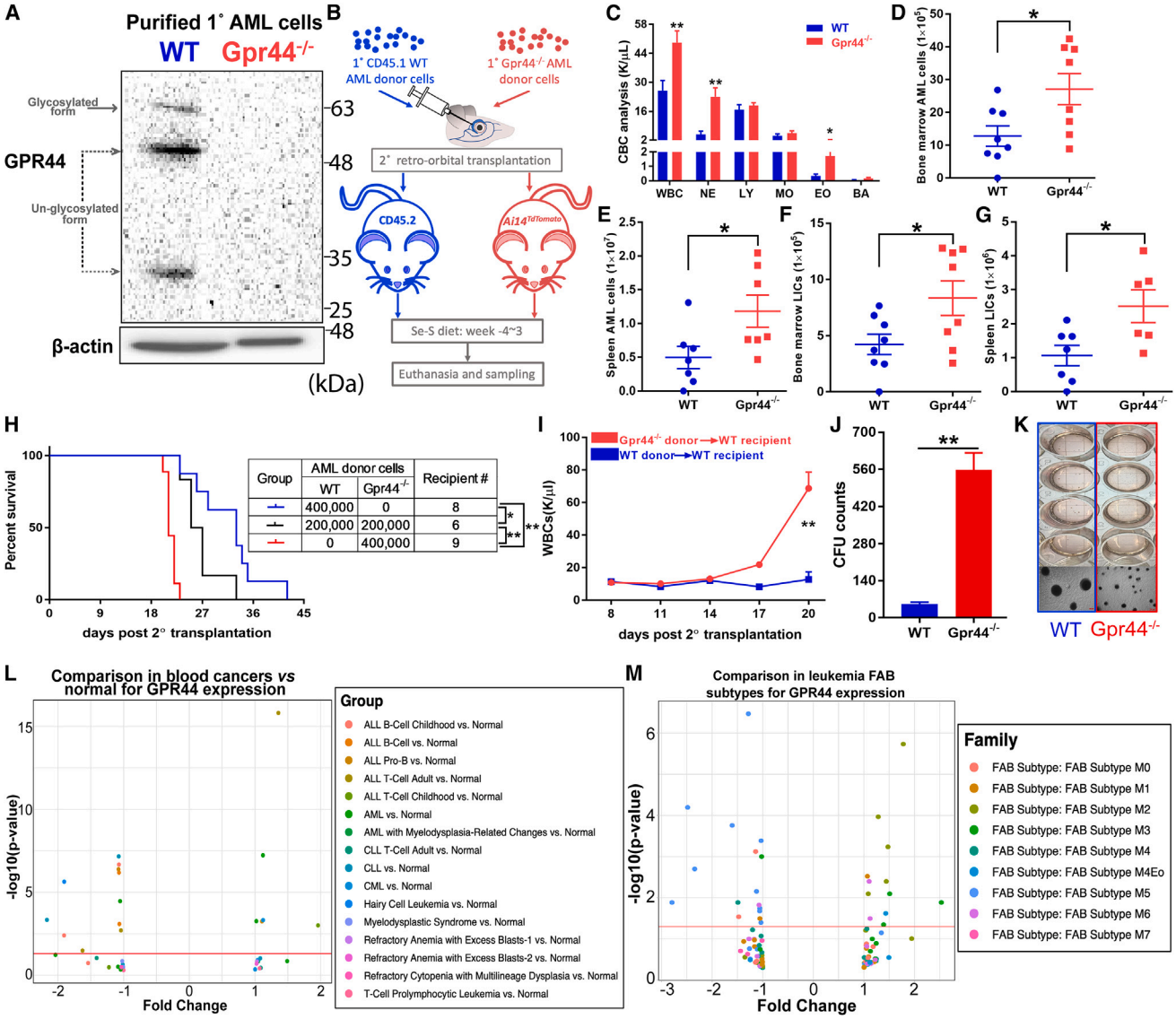

Figure 4. Lack of GPR44 in AML cells results in aggressive disease

(A) Western blot showing the expression of GPR44 and β-actin in purified 1° WT and *Gpr44*$^{-/-}$ AML cells. GPR44 antibody detects glycosylated (63 kDa) and un-glycosylated (33 and 50 kDa) and forms.

(B) CD45.2- and *Ai14*^{TdTomato}-recipient mice were maintained on Se-S diet for 4 weeks before transplantation until the endpoint. 2° transplantation was done retro-orbitally with 1° CD45.1 WT or CD45.2 Gpr44$^{-/-}$ AML donor cells to CD45.2= and *Ai14*^{TdTomato}-recipient mice, respectively; 3 weeks later, mice were euthanized; blood, bone marrow, and spleen were sampled (n = 8 in each group).

(C) CBC analysis of Se-S AML mice in (B).

(D and E) Counts of AML cells in the Lin^{-} population in the bone marrow (D) and spleen (E) of Se-S AML mice in (B).

(F and G) Counts of LICs (WT: CD45.1^{+}Lin^{-}Sca-1^{-}c-Kit^{+}, see also Figure S1J; Gpr44$^{-/-}$: RFP^{-}Lin^{-}Sca-1^{-}c-Kit^{+}, see also Figure S3K) in the bone marrow (F) and spleen (G) of Se-S AML mice in (B).

(H) Survival curve of recipient mice with competitive 2° transplantation of WT (4×10^5), WT + Gpr44$^{-/-}$ (2×10^5: 2×10^5), or Gpr44$^{-/-}$ (4×10^5) AML donor cells (n = 6–9 in each group).

(I) Progression of WBCs in the peripheral blood of recipient mice secondarily transplanted with WT or Gpr44$^{-/-}$ AML donor cells (n = 8–9 in each group).

(J) Purified 1° WT and Gpr44$^{-/-}$ AML cells were plated in methylcellulose medium (2,500 cells/well, 4 replicates). CFUs were counted on day 8.

(K) Representative image of colony growth from purified 1° WT and Gpr44$^{-/-}$ AML cells. Scale bar, 100 μm.

(L) Comparison of *GPR44* expression in blood cancers compared with normal subjects.

(M) Comparison of *GPR44* expression in AML FAB subtypes including M0, M1, M2, M3, M4, M4Eo, M5, M6, and M7.

(L and M) Data were generated from the ONCOMINE database. (L) Each point represents a comparison of the study between the cancer population and normal population. (M) Each point represents a comparison of the study of one FAB subtype with the other subtypes. Plots were generated using the –log10 (p value) and the fold change in expression. p values were obtained by t test of the mean values. An absolute fold change of 1.5 (red line) or higher is considered significant. Data shown are mean ± SEM per group; *$p < 0.05$, **$p < 0.01$.

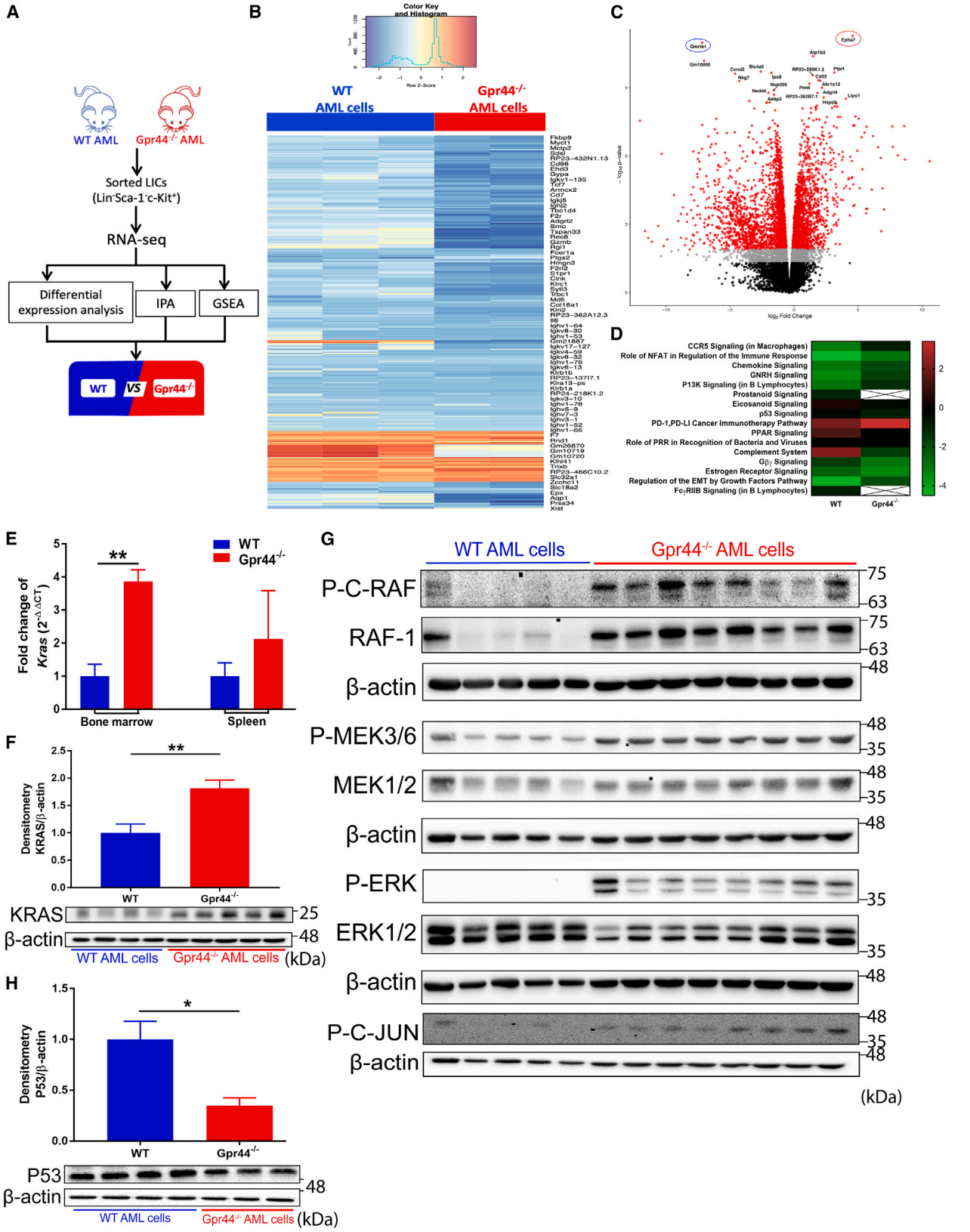

(legend on next page)

Deletion of GPR44 resulted in robust alteration of the transcriptional program (Figures 5B and 5C), which included multiple physiological gene sets (Figure S6A). Signaling pathways such as PPAR, P53, prostanoid, eicosanoid, and estrogen receptor signaling were significantly downregulated, while C-C motif chemokine receptor 5 (CCR5) signaling was upregulated in Gpr44$^{-/-}$ AML LICs (Figure 5D). We also identified multiple KRAS-upregulated gene signatures that were consistently expressed at higher levels in Gpr44$^{-/-}$ AML LICs (Figure S6B). Interestingly, mRNA and protein expression of Kras was significantly increased in both 2° and 1° Gpr44$^{-/-}$ AML cells compared with their WT AML cell controls (Figures 5E, 5F, S6C, and S6D). As expected, enhanced phosphorylation of MAPK components (RAF, MEK, and ERK) was seen in Gpr44$^{-/-}$ AML cells (Figure 5G) accompanied by increased expression of RAF-1. Increased expression of phosphorylated C-JUN, a downstream effector of MAPK signaling, further confirmed the activation of MAPK signaling in Gpr44$^{-/-}$ AML cells (Figure 5G) in agreement with the role of KRAS-MAPK signaling in leukemogenesis.[28–31] Downregulated P53 expression (Figure 5H) and associated gene signatures (Figure S6E) were also detected in Gpr44$^{-/-}$ AML cells that corroborated well with increased expression of pro-survival and anti-apoptotic genes (Figures S6F and S6G). NADPH oxidases (Nox), *Nox1*, *Nox2*, and *Nox3*, were also elevated in Gpr44$^{-/-}$ AML cells (Figure S6H), perhaps contributing to oxidative stress to favor leukemia.[32] Cell-cycle analysis indicated that most of the Gpr44$^{-/-}$ AML cells were in S and G2/M phases, showing a higher proliferation than WT AML cells (Figure S6I). In addition, increased expression of *Pdl1* and *Pd1* (Figure S6J) and their associated gene signatures (Figure S6K) and increased expression of Yes1-associated transcriptional regulator (*Yap1*), a key cell-cycle regulatory gene (Figure S6L), may partly explain the aggressiveness of Gpr44$^{-/-}$ AML cells.

Inhibition of KRAS/MAPK signaling reverses GPR44 KO-associated effect in AML

Treatment with BAY293, a potent KRAS inhibitor that disrupts the KRAS-SOS1 interaction, decreased the viability of Gpr44$^{-/-}$ AML cells in a dose- and time-dependent manner (Figures 6A, 6B, and S7A). To avoid any potential interference of <5% recipient cells, purified Gpr44$^{-/-}$ AML cells showed significantly decreased viability and cell number with BAY293 treatment (Figures 6C–6E) along with significantly decreased expression of anti-apoptotic genes and cell-cycle-associated genes (Figures S7B and S7C). Even a ~30% decrease in KRAS expression in Gpr44$^{-/-}$ AML cells using a lentiviral expression of dCas9-KRAB[33] and specific gRNA targeting mouse *Kras* promoter (Figures S7D and S7E) reduced the phosphorylated MEK3/6 and ERK (Figure 6F), and tertiary transplantation of such cells exhibited a significantly improved survival of the recipient mice (Figures 6G and 6H).

Gpr44$^{-/-}$ AML cells were treated *ex vivo* with a selective inhibitor of MEK, PD98059, followed by tertiary transplantation (Figure 6I), which increased survival of transplanted mice (Figure 6J). PD98059-treated Gpr44$^{-/-}$ AML cells showed decreased expression of P-ERK and increased P53 (Figure 6K) and attenuated expression of anti-apoptotic genes, cell-cycle-associated genes, and stem cell quiescence genes (Figures S7F–S7H). Inhibition of either KRAS or MEK impaired the colony-forming ability of Gpr44$^{-/-}$ AML cells (Figures 6L–6N). Altogether, these data demonstrate a previously unknown link between GPR44 regulation of KRAS/MAPK signaling, which could potentially serve as alternative targets to reverse exacerbation of AML in the absence of GPR44.

Deletion of GPR44 worsens AML by activation of PI3K/AKT/mTOR pathway

The involvement of KRAS with the PI3K/AKT/mTOR signaling pathway[34,35] was evaluated in WT and Gpr44$^{-/-}$ AML cells. *Pi3k* (*Pik3ca*, *Pik3cb*, and *Pi3kcd*) and *Akt* (*Akt1* and *Akt2*) (Figures 7A and 7B) were significantly upregulated in GPR44$^{-/-}$ AML cells, in addition to increased expression of *Pka* (*Prkca*, *Prkcb*, and *Prkcg*) and *Pkc* (*Prkacg*) (Figures 7C and 7D), while *Prkaca* and *Prkacb* were not expressed (not shown). Consistently, protein expression of PI3K, AKT, and mTOR and their phosphorylated forms was enhanced in purified 1° Gpr44$^{-/-}$ AML cells, and enhanced expression of P-P70-S6K in Gpr44$^{-/-}$ AML cells suggested that mTORC1 was activated (Figure 7E). However, expression of 4E-BP1 and P-4E-BP1 was decreased in Gpr44$^{-/-}$ AML cells despite the increase in mTORC1 (Figure 7F). The dramatic decrease in PTEN and P-PTEN suggested that the deletion of GPR44 could negatively impact the tumor suppressor role of PTEN in AML (Figure 7F). Use of chemical inhibitors of PI3K (LY294002 and Wortmannin) and mTORC (Sapanisertib and Torin1) led to decreased viability of Gpr44$^{-/-}$ AML cells (Figure 7G) in addition to the decreased

Figure 5. Lack of GPR44 activates KRAS-MAPK signaling in AML cells

(A) Scheme for sequencing analysis. Bone marrow cells were isolated from mice secondarily transplanted with 1° WT or Gpr44$^{-/-}$ AML donor cells and LICs were flow cytometrically sorted following RBC lysis, Lin$^-$ selection, and Sca-1 and c-Kit staining. LICs (4×10^5) were used for RNA sequencing. Differential gene expression analysis, IPA, and GSEA were performed to compare WT and Gpr44$^{-/-}$ LICs (n = 3 in each group).

(B) Heatmap for top 100 most differentially regulated genes in WT and Gpr44$^{-/-}$ LICs.

(C) Volcano plot for differential gene expression analysis between WT and Gpr44$^{-/-}$ LICs.

(D) Heatmap of indicated pathways in WT and Gpr44$^{-/-}$ LICs as analyzed by IPA. *Z* scores were plotted.

(E) Expression of *Kras* assessed by qPCR analysis in WT or Gpr44$^{-/-}$ AML cells isolated from bone marrow (left) and spleen (right) of 2° AML-recipient mice. Data were normalized to WT AML cells and *18S* rRNA expression (n = 4–8 biological replicates).

(F) Western blot showing the expression of KRAS in WT or Gpr44$^{-/-}$ AML cells isolated from 2° AML-recipient mice.

(G) Western blot showing the expression of MAPK signaling pathway components including P-C-RAF, RAF-1, P-MEK3/6, MEK1/2, P-ERK, ERK1/2, P-C-JUN, and β-actin in WT or Gpr44$^{-/-}$ AML cells isolated from 2° AML-recipient mice (n = 5–8 biological replicates in each group).

(H) Western blot showing the expression of P53 in WT or Gpr44$^{-/-}$ AML cells isolated from 2° AML-recipient mice. (F and H) Densitometry was done by normalizing to WT AML cells and relative to β-actin (n = 3–5 biological replicates in each group).

Data shown are mean ± SEM per group; *$p < 0.05$, **$p < 0.01$.

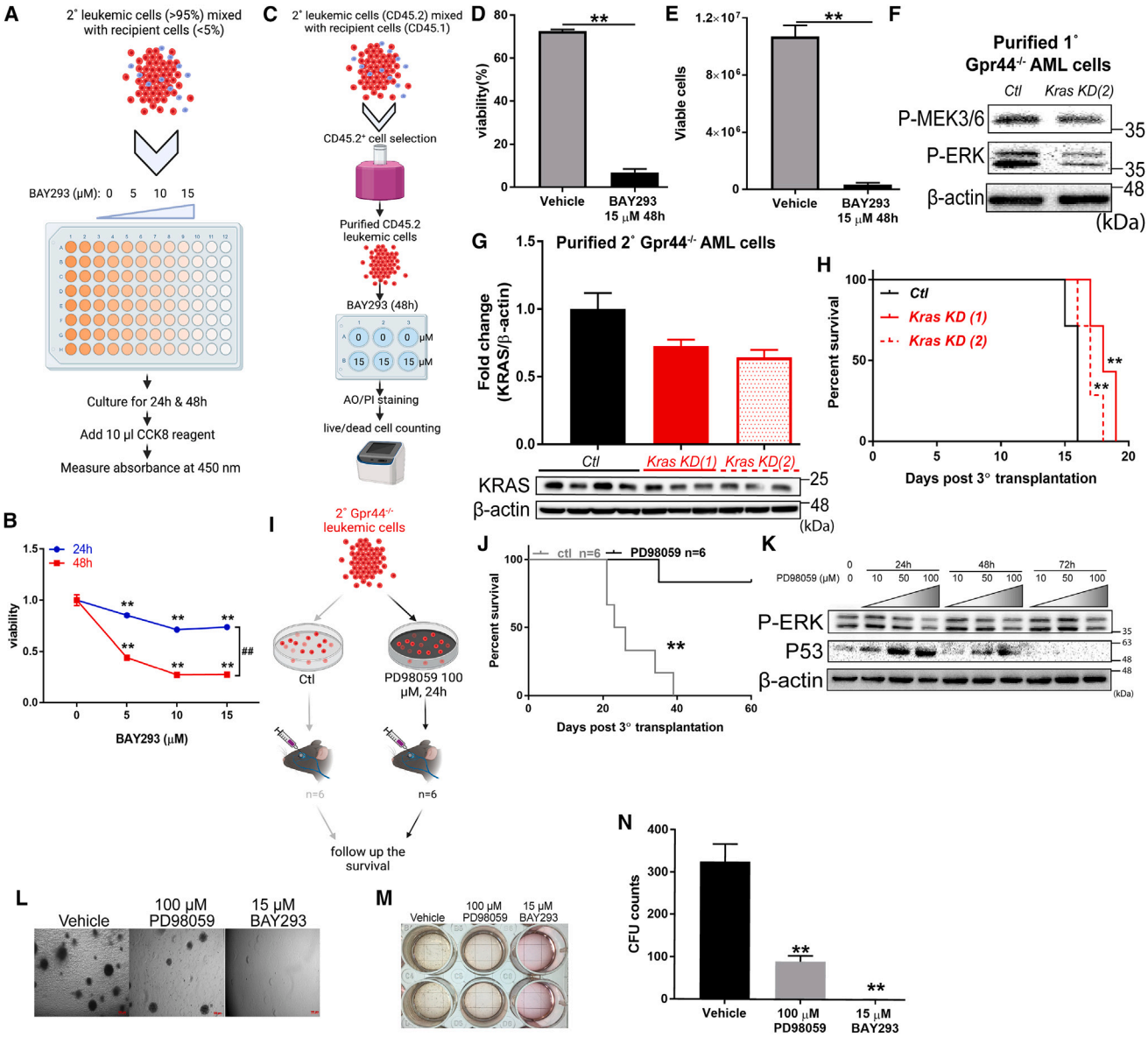

Figure 6. Inhibition of KRAS/MAPK signaling reverses GPR44 KO-associated effect in AML

(A) Scheme showing the treatment of BAY293 and CCK8 assay on unpurified Gpr44$^{-/-}$ AML cells. Frequency of AML cells was above 95%.

(B) Comparison of the viability of unpurified Gpr44$^{-/-}$ AML cells treated with BAY293 (0, 5, 10, and 15 μM, n = 3) for 24 or 48 h. Data were normalized to 0 μM (24 h) treatment. **$p < 0.01$, comparison between concentrations in the 24 and 48 h time points analyzed by Student's t test; $^{##}p < 0.01$, comparison between time points analyzed by two-way ANOVA followed by appropriate post hoc test (Bonferroni correction).

(C) Scheme showing the treatment of BAY293 and live/dead cell measurement on purified Gpr44$^{-/-}$ AML cells. CD45.2 Gpr44$^{-/-}$ AML cells were transplanted into CD45.1 recipients; purification of Gpr44$^{-/-}$ AML cells isolated from spleen was done by CD45.1-positive magnet selection kit.

(D and E) Frequency (D) and count (E) of live cells in purified Gpr44$^{-/-}$ AML cells treated with 15 μM BAY293 for 48 h (n = 3).

(F) Western blot showing the expression of P-MEK3/6 and P-ERK in purified 1° Gpr44$^{-/-}$ AML cells transduced with pLV hU6-sgRNA KRAS hUbC-dCas9-KRAB-T2a-GFP virus.

(G) Western blot showing the expression of KRAS in purified 2° Gpr44$^{-/-}$ AML cells transduced with pLV hU6-sgRNA KRAS hUbC-dCas9-KRAB-T2a-GFP virus. Densitometry was done by normalizing to control group and relative to β-actin (n = 3–4 in each group).

(H) Survival curve of AML mice tertiarily transplanted with purified *KRAS KD* Gpr44$^{-/-}$ AML cells (n = 7).

(I and J) Survival analysis of mice tertiarily transplanted PD98059-treated Gpr44$^{-/-}$ AML cells. Gpr44$^{-/-}$ AML cells were cultured *ex vivo* with or without 100 μM PD98059 for 24 h and then retro-orbitally transplanted into mice (n = 6 per group). Survival was followed up for 60 days post transplantation.

(K) Western blot showing the expression of P-ERK and P53 in Gpr44$^{-/-}$ AML cells treated with PD98059 (0, 10, 50, and 100 μM) for 24, 48, and 72 h.

(legend continued on next page)

CellPress
OPEN ACCESS

phosphorylation of P70-S6K, further validating the role of the PI3K/AKT/mTOR pathway (Figure 7H). However, the expression of P-4E-BP1 was also unexpectedly decreased by Wortmannin, Sapanisertib, and Torin 1 (Figure 7I). Use of LY294002, Sapanisertib, and LY258470002 (P70-S6K inhibitor) significantly inhibited the colony-forming ability, suggesting that PI3K was highly expressed and activated in Gpr44$^{-/-}$ AML cells (Figures 7J and 7K).

Lack of GPR44 enhances expression of RTKs

In the case of WT AML cells, a 2-fold higher level of intracellular cAMP was seen when compared with Gpr44$^{-/-}$ AML cells, suggesting involvement of $G_{\alpha s}$ (Figure S8A), which is contrary to existing data on Gpr44 signaling in other cell types.[36] Consistently, cAMP responsive gene signatures (Figure S8B), as well as the activation (phosphorylation) and expression of cAMP-response element binding protein (Figure S8C) were also decreased in Gpr44$^{-/-}$ AML cells, suggesting that downstream signaling events, including decreased cAMP, induced by GPR44 deletion, upregulated KRAS activity.

GSEA revealed that gene sets targeted by mir512-5p, mir143, and Let-7 were highly enriched in WT AML cells but not in Gpr44$^{-/-}$ AML LICs (Figure S8D). qRT-PCR confirmed a significant downregulation of *Mir143* in Gpr44$^{-/-}$ AML cells (Figure S8E). *Mir143* also showed a dose-dependent enhancement in WT AML cells isolated from AML mice on Na_2SeO_3-supplemented diets (Figure S8F). Considering their reported inhibitory effect on the expression of KRAS,[37–40] it is likely that GPR44 deletion enhances the expression of KRAS via downregulating these miRNAs in AML cells. Similar mechanisms may underlie the enhanced expression of RAF, PI3K, AKT, mTOR, and P70-S6K in GPR44$^{-/-}$ AML cells. However, the increased activity (phosphorylation) of both MAPK and PI3K/AKT/mTOR signaling pathways hinted that KRAS activity was also elevated along with the upregulation of its expression. Since KRAS can be activated by multiple upstream signals, such as activation of RTKs in other cancers,[41] we investigated the expression of growth factors and their receptors in WT and Gpr44$^{-/-}$ AML LICs from our RNA-seq dataset. Several receptors, including Kit, Flt3, Epha7, Hdgfrp3, and Pdgfrb, were expressed at a higher level in Gpr44$^{-/-}$ AML LICs than WT AML LICs (Figure S8G). Consistently, increased EPHA7, EGFR, and FLT3 was also seen at the protein level (Figure S8H) in Gpr44$^{-/-}$ AML cells. TGFBR III was induced upon GPR44 deletion in AML cells, whereas TGFBR II was decreased (Figure S8H). On the other hand, we failed to detect a corresponding increase in membrane PDGFRB (Figure S8I); and CP-673451, a specific PDGFRB inhibitor, did not affect the viability of Gpr44$^{-/-}$ AML cells (Figure S8J). However, imatinib, a general RTK inhibitor marginally reduced the viability of Gpr44$^{-/-}$ AML cells at high concentrations, suggesting a broad activation of RTKs (FLT3, EGFR, and EPHA7) when signals from GPR44 are cut off (Figure S8K).

DISCUSSION

In our study, activation of GPR44 led to apoptosis in both AML and CML LICs in murine models of human leukemia, human AML cell lines, and patient samples. We observed this effect when Gpr44 was activated by endogenous CyPGs produced following dietary Se supplementation (through the COX-H-PGDS pathway) or by treatment with exogenous CyPGs. Deletion of GPR44 in AML mice exacerbated the disease via upregulation of RTK-associated KRAS-mediated MAPK and PI3K/AKT/mTOR signaling pathways. Importantly, our studies suggested a crosstalk between PPARγ and GPR44 and activation of pro-apoptotic pathways, but that crosstalk was not always essential. CyPGs had no impact on normal HSCs in the bone marrow of AML or CML mice, making this a safe treatment regimen that may also ensure efficient convalescent recovery of normal hematopoiesis during leukemia.

Even though the health effects of Se deficiency or Se excess are well known in prostate cancer following the SELECT trial, the beneficial effects of Se supplementation generally favor those deficient in Se.[42,43] In contrast to our findings, a recent study found that a Se-D diet fed post transplantation improved survival of MLL-AF9-induced AML mice.[44] Such an effect could be due to exacerbated oxidative stress leading to the ablation of leukemia cells, a possibility underlying the U-shaped association between Se status and cancer risk.[45] However, Se supplementation could mitigate collateral effects of inflammation in addition to targeting tumor cells. That said, the ideal form of Se for dietary supplementation, either inorganic selenite or organic SeMet, continues to be debated. Selenite is rapidly absorbed at a higher efficiency than SeMet. In addition to being nonspecifically incorporated into proteins, SeMet is metabolized by cystathionine gamma-lyase to form selenide that is incorporated as Sec into selenoproteins.[46] SeMet did not compare well with selenite in our study due, in part, to the decreased COX-1/H-PGDS expression that impacted CyPG production. Previously, we showed that selenite decreased the expression of 15-hydroxyprostaglandin dehydrogenase (15-PGDH), an enzyme that catalyzes the oxidation of the hydroxyl group in many bioactive lipid mediators, including CyPGs,[47] in CML mice,[15] whereas SeMet is reported to induce the expression of 15-PGDH.[48] Such a differential regulation of 15-PGDH expression by selenite and SeMet may indicate divergent mechanisms that could also dictate the beneficial effect of Se in AML.

GPR44 activation by PGD_2 was originally reported to mediate chemotaxis in eosinophils, basophils, and Th2 cells in allergy and asthma.[18,19,49–52] The role of GPR44 in gastric cancer,[53,54] colorectal cancer,[55] and prostate cancer[56] suggested that the pro-tumorigenic effect was focused on its role in the microenvironment comprised of innate lymphoid-like cells (ILC2), Tregs, and myeloid-derived suppressor cells, which support an immunosuppressive niche.[56,57] In two gastric cancer cell lines, HGC-27 and SGC-7901, PGD_2/GPR44 signaling restricted their

(L and M) Representative image of colony growth from purified 2° Gpr44$^{-/-}$ AML cells (2,500 cells/well, n = 4 for biological replicate, n = 2 for technical replicate) treated with 100 μM PD98059 and 15 μM BAY293 in methylcellulose medium. Scale bar, 100 μm.

(N) Counts of CFUs from purified 2° Gpr44$^{-/-}$ AML cells treated with 100 μM PD98059 and 15 μM BAY293 in methylcellulose medium. CFUs were counted on day 8.

Data shown are mean ± SEM per group; *$p < 0.05$, ** $p < 0.01$.

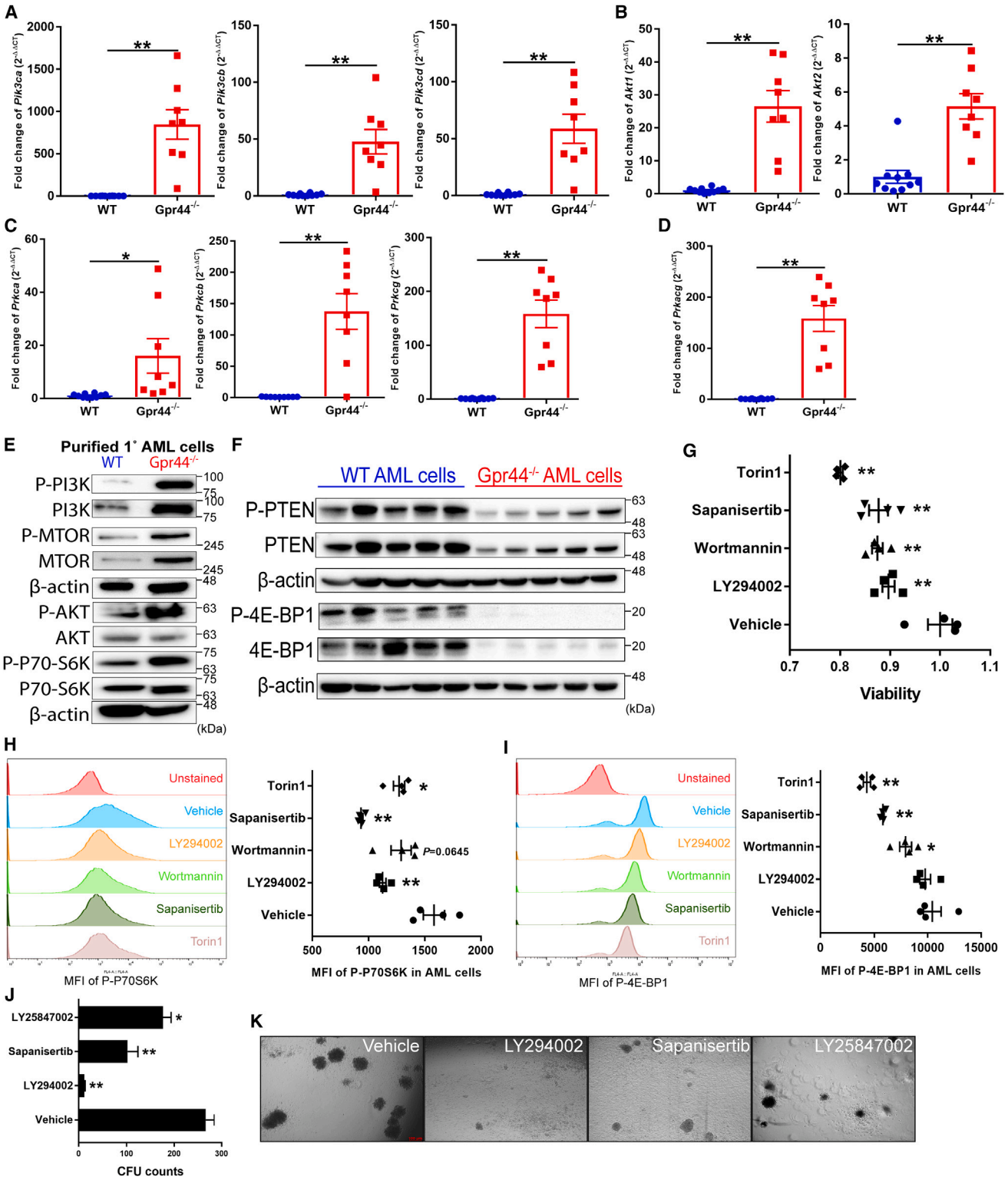

Figure 7. Deletion of GPR44 worsens AML by activation of the PI3K/AKT/mTOR pathway

(A–D) Expression of genes including PI3K (*Pik3ca*, *Pik3cb*, *Pik3cd*) (A), AKT (*Akt1*, *Akt2*) (B), PKC (*Prkca*, *Prkcb*, *Prkcg*) (C), and PKA (*Prkacg*) (D) assessed by qPCR analysis in WT or *Gpr44*$^{-/-}$ AML cells isolated from spleens of 2° AML-recipient mice. Data were normalized to WT AML cells and Gapdh expression (n = 8–10 biological replicates in each group).

(legend continued on next page)

self-renewal and increased cell differentiation *in vitro* while inhibiting tumorigenesis, tumor growth, and metastasis *in vivo*,[58] which corroborates our results in primary LICs. Clearly, cell membrane expression of GPR44 on tumor cells is of importance to the therapeutic targeting by CyPGs. Even though internalized GPCRs can signal,[59] it is clear that, unlike the various patient cells that responded to DK-PGD$_2$, signaling from internalized GPR44 in MOLM13 cells, if any, needs to be further characterized to provide alternative mechanisms. Thus, the correlation of GPR44 expression with the survival of AML patients needs to be conducted within a larger and stratified population to further explore the clinical importance of GPR44-based therapies.

Mutations within RTKs (EPHA7, EGFR, and FLT3), KRAS-MAPK, and PI3K/AKT/mTOR pathways are frequently described in various cancers,[60–63] which were also observed in our study. However, K562 cells, which contain a BCR-ABL fusion, and SEMK2 cells, which contain an MLL-AF4 fusion, exhibit induced deregulation of EPHA7 and ERK phosphorylation, suggesting a functional discrepancy between primary stem cells and immortalized cell lines.[64] Regardless, the ability to modulate these upstream pathways by GPR44 opens another window of opportunity to target cancer cells.

Limitations of the study

Given that AML is a complex heterogeneous disease, we acknowledge the possibility that Se or CyPGs may not induce complete remission in patients. Thus, further studies are needed to demonstrate the efficacy of Se and/or CyPGs in AML with mutations other than MLL-AF9, and studies in humanized models where patient-derived xenografts are used in NSG mice would further facilitate an efficient translation to the clinic. Our studies also raise an important question regarding the role of GPR44 in P53-independent mechanisms of apoptosis, particularly in cells with P53 mutations. Further characterization of such signaling complexities would be necessary. Even though our studies suggest some level of control of GPR44 signaling pathways by miRNAs, further characterization of the underlying mechanisms is needed. Finally, attenuation of AML by inhibition of glutathione peroxidase 1 or genetic deletion of selenophosphate synthetase 2 (*SEPHS2*) contradicts the protective efficacy of Se supplementation in cancers, while supporting a better outcome in Se-deficient rodent models.[44,65,66] The exact role of Se and specific selenoproteins in LICs versus those in the tumor microenvironment could also open new pathways for direct dietary modulation leading to endogenous production of CyPGs.

STAR★METHODS

Detailed methods are provided in the online version of this paper and include the following:

- KEY RESOURCES TABLE
- RESOURCE AVAILABILITY
  - Lead contact
  - Materials availability
  - Data and code availability
- EXPERIMENTAL MODEL AND SUBJECT PARTICIPANT DETAILS
  - Cell cultures
  - Experimental animals
  - Generation of *Gpr44*$^{-/-}$ mice
  - Lentivirus cloning and production
  - Generation of experimental murine models of AML and CML
- METHOD DETAILS
  - Serial transplantation and survival analyses
  - Purification of AML cells
  - Dietary treatments
  - In-vivo inhibition of H-PGDS
  - In-vivo treatment of CyPGs
  - In-vivo modulation of PPARγ
  - In-vitro treatment of Na_2SeO_3
  - In-vitro treatment of CyPGs
  - In-vitro inhibition of KRAS
  - In-vitro knockdown of KRAS via CRISPRi
  - In-vitro inhibition of ERK
  - In-vitro inhibition of PI3K, AKT, and MTORC
  - In-vitro inhibition of RTKs and PDGFR
  - Methylcellulose culture
  - Measurement of 15d-PGJ$_2$ by enzyme-linked immunoassay (ELISA)
  - Measurement of cyclic adenosine monophosphate (cAMP) by ELISA
  - Measurement of apoptosis
  - Measurement of cell cycle
  - FACS analysis
  - Western immunoblotting
  - qPCR
  - RNAseq analysis
  - Gene set enrichment analysis (GSEA)
  - Ingenuity pathway analysis (IPA)
  - ONCOMINE analysis

(E) Western blot showing the expression of Phospho-PI3K, PI3K, Phospho-mTOR, mTOR, Phospho-AKT, AKT, Phospho-P70-S6K, P70-S6K, and β-actin in purified 1° WT and Gpr44$^{-/-}$ AML cells.
(F) Western blot showing the expression of Phospho-PTEN, PTEN, Phospho-4EBP1, 4EBP1, and β-actin in WT or Gpr44$^{-/-}$ AML cells isolated from spleens of 2° AML-recipient mice (n = 5 biological replicates in each group).
(G) Viability of purified 1° Gpr44$^{-/-}$ AML cells treated with 150 μM ARN509, 10 μM LY294002, 10 nM Wortmannin, 10 nM Sapanisertib, 250 nM Torin1 for 24 h. Data were normalized and compared with vehicle treatment.
(H and I) Flow cytometric analysis of Phospho-P70-S6K (H) and Phospho-4E-BP1 (I) in CD45.1$^+$ 1° Gpr44$^{-/-}$ AML cells treated with 10 μM LY294002, 10 nM Wortmannin, 10 nM Sapanisertib, 250 nM Torin1 for 24 h. MFI was summarized (n = 4).
(J) Counts of CFUs of purified 1° Gpr44$^{-/-}$ AML cells treated with 10 μM LY294002, 10 nM Sapanisertib, and 2.5 μM LY2584702 in methylcellulose medium (2,500 cells/well, n = 3 for technical replicate) CFUs were counted on day 8.
(K) Representative image of colony growth in (J). Scale bar, 100 μm.
Data shown are mean ± SEM per group; *p < 0.05, **p < 0.01.

- Hematology
- Biochemistry analysis
- Histological analysis
- Radioligand binding assay

- QUANTIFICATION AND STATISTICAL ANALYSIS

SUPPLEMENTAL INFORMATION

Supplemental information can be found online at https://doi.org/10.1016/j.celrep.2023.112794.

ACKNOWLEDGMENTS

We thank Brian Dawson and Sarah Neering at the Flow Cytometry Core Facility of Penn State Huck Institutes of the Life Sciences for cell sorting and current and former members in Prabhu and Paulson laboratories for timely help. We acknowledge the contributions of our colleagues from the Animal Resource Program at Penn State. This work was supported, in part, by grants from the American Institute for Cancer Research, NIH R01DK077152, UDSA-NIFA Hatch project (no. 4771, accession no. 0000005) to K.S.P. and R.F.P.

AUTHOR CONTRIBUTIONS

Research design, F.Q., K.S.P., and R.F.P.; investigation, F.Q., S.K.N., B.E.A., D.B.T., D.S., S.H., U.H.G., E.R.F., L.G., and M.D.Q.; data processing and analysis, F.Q. and J.Z.; human sample collection, C.A., A.S., and D.F.C.; writing, F.Q., K.S.P., and R.F.P.; draft editing, all authors.

DECLARATION OF INTERESTS

K.S.P. and R.F.P. have ownership interest (including patents) in OncOmega Inc. and Nemean Pharma Corporation.

Received: July 22, 2022
Revised: March 25, 2023
Accepted: June 27, 2023
Published: July 18, 2023

REFERENCES

1. Norris, D., and Stone, J. (2008). WHO Classification of Tumours of Haematopoietic and Lymphoid Tissues (Geneva: WHO).
2. Döhner, H., Weisdorf, D.J., and Bloomfield, C.D. (2015). Acute myeloid leukemia. N. Engl. J. Med. *373*, 1136–1152. https://doi.org/10.1056/NEJMra1406184.
3. De Kouchkovsky, I., and Abdul-Hay, M. (2016). Acute myeloid leukemia: a comprehensive review and 2016 update. Blood Cancer J. *6*, e441. https://doi.org/10.1038/bcj.2016.50.
4. Kern, W., Voskova, D., Schoch, C., Hiddemann, W., Schnittger, S., and Haferlach, T. (2004). Determination of relapse risk based on assessment of minimal residual disease during complete remission by multiparameter flow cytometry in unselected patients with acute myeloid leukemia. Blood *104*, 3078–3085. https://doi.org/10.1182/blood-2004-03-1036.
5. Feller, N., van der Pol, M.A., van Stijn, A., Weijers, G.W.D., Westra, A.H., Evertse, B.W., Ossenkoppele, G.J., and Schuurhuis, G.J. (2004). MRD parameters using immunophenotypic detection methods are highly reliable in predicting survival in acute myeloid leukaemia. Leukemia *18*, 1380–1390. https://doi.org/10.1038/sj.leu.2403405.
6. van Rhenen, A., Feller, N., Kelder, A., Westra, A.H., Rombouts, E., Zweegman, S., van der Pol, M.A., Waisfisz, Q., Ossenkoppele, G.J., and Schuurhuis, G.J. (2005). High stem cell frequency in acute myeloid leukemia at diagnosis predicts high minimal residual disease and poor survival. Clin. Cancer Res. *11*, 6520–6527. https://doi.org/10.1158/1078-0432.CCR-05-0468.
7. Reya, T., Morrison, S.J., Clarke, M.F., and Weissman, I.L. (2001). Stem cells, cancer, and cancer stem cells. Nature *414*, 105–111. https://doi.org/10.1038/35102167.
8. Weisberger, A.S., and Suhrland, L.G. (1956). Studies on analogues of L-cysteine and L-cystine: III. The effect of selenium cystine on leukemia. Blood *11*, 19–30. https://doi.org/10.1182/blood.V11.1.19.19.
9. Batist, G., Katki, A.G., Klecker, R.W., and Myers, C.E. (1986). Selenium-induced cytotoxicity of human leukemia cells: interaction with reduced glutathione. Cancer Res. *46*, 5482–5485.
10. Philchenkov, A., Zavelevich, M., Khranovskaya, N., and Surai, P. (2007). Comparative analysis of apoptosis induction by selenium compounds in human lymphoblastic leukemia MT-4 cells. Exp. Oncol. *29*, 257–261.
11. Li, J., Zuo, L., Shen, T., Xu, C.-m., and Zhang, Z.-n. (2003). Induction of apoptosis by sodium selenite in human acute promyelocytic leukemia NB4 cells: involvement of oxidative stress and mitochondria. J. Trace Elem. Med. Biol. *17*, 19–26. https://doi.org/10.1016/S0946-672X(03)80041-X.
12. Gandhi, U.H., Kaushal, N., Hegde, S., Finch, E.R., Kudva, A.K., Kennett, M.J., Jordan, C.T., Paulson, R.F., and Prabhu, K.S. (2014). Selenium suppresses leukemia through the action of endogenous eicosanoids. Cancer Res. *74*, 3890–3901. https://doi.org/10.1158/0008-5472.CAN-13-3694.
13. Nelson, S.M., Lei, X., and Prabhu, K.S. (2011). Selenium levels affect the IL-4–induced expression of alternative activation markers in murine macrophages. J. Nutr. *141*, 1754–1761. https://doi.org/10.3945/jn.111.141176.
14. Gandhi, U.H., Kaushal, N., Ravindra, K.C., Hegde, S., Nelson, S.M., Narayan, V., Vunta, H., Paulson, R.F., and Prabhu, K.S. (2011). Selenoprotein-dependent up-regulation of hematopoietic prostaglandin D2 synthase in macrophages is mediated through the activation of peroxisome proliferator-activated receptor (PPAR) γ. J. Biol. Chem. *286*, 27471–27482. https://doi.org/10.1074/jbc.M111.260547.
15. Finch, E.R., Tukaramrao, D.B., Goodfield, L.L., Quickel, M.D., Paulson, R.F., and Prabhu, K.S. (2017). Activation of PPARgamma by endogenous prostaglandin J(2) mediates the antileukemic effect of selenium in murine leukemia. Blood *129*, 1802–1810. https://doi.org/10.1182/blood-2016-08-736405.
16. Qian, F., Arner, B.E., Kelly, K.M., Annageldiyev, C., Sharma, A., Claxton, D.F., Paulson, R.F., and Prabhu, K.S. (2022). Interleukin-4 treatment reduces leukemia burden in acute myeloid leukemia. FASEB J *36*, e22328. https://doi.org/10.1096/fj.202200251R.
17. Jandl, K., and Heinemann, A. (2017). The therapeutic potential of CTRTH2/DP2 beyond allergy and asthma. Prostaglandins Other Lipid Mediat. *133*, 42–48. https://doi.org/10.1016/j.prostaglandins.2017.08.006.
18. Hirai, H., Tanaka, K., Yoshie, O., Ogawa, K., Kenmotsu, K., Takamori, Y., Ichimasa, M., Sugamura, K., Nakamura, M., Takano, S., and Nagata, K. (2001). Prostaglandin D2 selectively induces chemotaxis in T helper type 2 cells, eosinophils, and basophils via seven-transmembrane receptor CRTH2. J. Exp. Med. *193*, 255–261. https://doi.org/10.1084/jem.193.2.255.
19. Nagata, K., and Hirai, H. (2003). The second PGD(2) receptor CRTH2: structure, properties, and functions in leukocytes. Prostaglandins Leukot. Essent. Fatty Acids *69*, 169–177. https://doi.org/10.1016/s0952-3278(03)00078-4.
20. Pettipher, R., Hansel, T.T., and Armer, R. (2007). Antagonism of the prostaglandin D2 receptors DP1 and CRTH2 as an approach to treat allergic diseases. Nat. Rev. Drug Discov. *6*, 313–325. https://doi.org/10.1038/nrd2266.
21. Matsuo, Y., MacLeod, R.A., Uphoff, C.C., Drexler, H.G., Nishizaki, C., Katayama, Y., Kimura, G., Fujii, N., Omoto, E., Harada, M., and Orita, K. (1997). Two acute monocytic leukemia (AML-M5a) cell lines (MOLM-13 and MOLM-14) with interclonal phenotypic heterogeneity showing MLL-AF9 fusion resulting from an occult chromosome insertion, ins(11;9)(q23;p22p23). Leukemia *11*, 1469–1477. https://doi.org/10.1038/sj.leu.2400768.
22. Aritake, K., Kado, Y., Inoue, T., Miyano, M., and Urade, Y. (2006). Structural and functional characterization of HQL-79, an orally selective inhibitor

of human hematopoietic prostaglandin D synthase. J. Biol. Chem. *281*, 15277–15286. https://doi.org/10.1074/jbc.M506431200.

23. Kaushal, N., Kudva, A.K., Patterson, A.D., Chiaro, C., Kennett, M.J., Desai, D., Amin, S., Carlson, B.A., Cantorna, M.T., and Prabhu, K.S. (2014). Crucial role of macrophage selenoproteins in experimental colitis. J. Immunol. *193*, 3683–3692. https://doi.org/10.4049/jimmunol.1400347.
24. Rangachari, P.K., and Betti, P.A. (1993). Biological activity of metabolites of PGD2 on canine proximal colon. Am. J. Physiol. *264*, G886–G894. https://doi.org/10.1152/ajpgi.1993.264.5.G886.
25. Hegde, S., Kaushal, N., Ravindra, K.C., Chiaro, C., Hafer, K.T., Gandhi, U.H., Thompson, J.T., van den Heuvel, J.P., Kennett, M.J., Hankey, P., et al. (2011). Delta12-prostaglandin J3, an omega-3 fatty acid-derived metabolite, selectively ablates leukemia stem cells in mice. Blood *118*, 6909–6919. https://doi.org/10.1182/blood-2010-11-317750.
26. Forman, B.M., Tontonoz, P., Chen, J., Brun, R.P., Spiegelman, B.M., and Evans, R.M. (1995). 15-deoxy-Δ12, 14-prostaglandin J2 is a ligand for the adipocyte determination factor PPARγ. Cell *83*, 803–812. https://doi.org/10.1016/0092-8674(95)90193-0.
27. Kliewer, S.A., Lenhard, J.M., Willson, T.M., Patel, I., Morris, D.C., and Lehmann, J.M. (1995). A prostaglandin J2 metabolite binds peroxisome proliferator-activated receptor gamma and promotes adipocyte differentiation. Cell *83*, 813–819. https://doi.org/10.1016/0092-8674(95)90194-9.
28. Seger, R., and Krebs, E.G. (1995). Protein Kinases .7. The Mapk Signaling Cascade. Faseb. J. *9*, 726–735.
29. Zhang, X.F., Settleman, J., Kyriakis, J.M., Takeuchi-Suzuki, E., Elledge, S.J., Marshall, M.S., Bruder, J.T., Rapp, U.R., and Avruch, J. (1993). Normal and oncogenic p21ras proteins bind to the amino-terminal regulatory domain of c-Raf-1. Nature *364*, 308–313. https://doi.org/10.1038/364308a0.
30. Kim, S.C., Hahn, J.S., Min, Y.H., Yoo, N.C., Ko, Y.W., and Lee, W.J. (1999). Constitutive activation of extracellular signal-regulated kinase in human acute leukemias: combined role of activation of MEK, hyperexpression of extracellular signal-regulated kinase, and downregulation of a phosphatase. Blood *93*, 3893–3899. https://doi.org/10.1182/blood.V93.11.3893.
31. Towatari, M., Iida, H., Tanimoto, M., Iwata, H., Hamaguchi, M., and Saito, H. (1997). Constitutive activation of mitogen-activated protein kinase pathway in acute leukemia cells. Leukemia *11*, 479–484. https://doi.org/10.1038/sj.leu.2400617.
32. Trombetti, S., Cesaro, E., Catapano, R., Sessa, R., Lo Bianco, A., Izzo, P., and Grosso, M. (2021). Oxidative Stress and ROS-Mediated Signaling in Leukemia: Novel Promising Perspectives to Eradicate Chemoresistant Cells in Myeloid Leukemia. Int. J. Mol. Sci. *22*, 2470. https://doi.org/10.3390/ijms22052470.
33. Thakore, P.I., D'Ippolito, A.M., Song, L., Safi, A., Shivakumar, N.K., Kabadi, A.M., Reddy, T.E., Crawford, G.E., and Gersbach, C.A. (2015). Highly specific epigenome editing by CRISPR-Cas9 repressors for silencing of distal regulatory elements. Nat. Methods *12*, 1143–1149. https://doi.org/10.1038/nmeth.3630.
34. Repasky, G.A., Chenette, E.J., and Der, C.J. (2004). Renewing the conspiracy theory debate: does Raf function alone to mediate Ras oncogenesis? Trends Cell Biol. *14*, 639–647. https://doi.org/10.1016/j.tcb.2004.09.014.
35. Rodriguez-Viciana, P., Warne, P.H., Dhand, R., Vanhaesebroeck, B., Gout, I., Fry, M.J., Waterfield, M.D., and Downward, J. (1994). Phosphatidylinositol-3-OH kinase as a direct target of Ras. Nature *370*, 527–532. https://doi.org/10.1038/370527a0.
36. Sawyer, N., Cauchon, E., Chateauneuf, A., Cruz, R.P.G., Nicholson, D.W., Metters, K.M., O'Neill, G.P., and Gervais, F.G. (2002). Molecular pharmacology of the human prostaglandin D2 receptor, CRTH2. Br. J. Pharmacol. *137*, 1163–1172. https://doi.org/10.1038/sj.bjp.0704973.
37. Forzati, F., De Martino, M., Esposito, F., Sepe, R., Pellecchia, S., Malapelle, U., Pellino, G., Arra, C., and Fusco, A. (2017). miR-155 is positively regulated by CBX7 in mouse embryonic fibroblasts and colon carcinomas, and targets the KRAS oncogene. BMC Cancer *17*, 170–179. https://doi.org/10.1186/s12885-017-3158-z.
38. Johnson, S.M., Grosshans, H., Shingara, J., Byrom, M., Jarvis, R., Cheng, A., Labourier, E., Reinert, K.L., Brown, D., and Slack, F.J. (2005). RAS is regulated by the let-7 microRNA family. Cell *120*, 635–647. https://doi.org/10.1016/j.cell.2005.01.014.
39. Takai, T., Tsujino, T., Yoshikawa, Y., Inamoto, T., Sugito, N., Kuranaga, Y., Heishima, K., Soga, T., Hayashi, K., Miyata, K., et al. (2019). Synthetic miR-143 Exhibited an Anti-Cancer Effect via the Downregulation of K-RAS Networks of Renal Cell Cancer Cells In Vitro and In Vivo. Mol. Ther. *27*, 1017–1027. https://doi.org/10.1016/j.ymthe.2019.03.004.
40. Spierings, D.C., McGoldrick, D., Hamilton-Easton, A.M., Neale, G., Murchison, E.P., Hannon, G.J., Green, D.R., and Withoff, S. (2011). Ordered progression of stage-specific miRNA profiles in the mouse B2 B-cell lineage. Blood *117*, 5340–5349. https://doi.org/10.1182/blood-2010-10-316034.
41. Marshall, C.J. (1995). Specificity of receptor tyrosine kinase signaling: transient versus sustained extracellular signal-regulated kinase activation. Cell *80*, 179–185. https://doi.org/10.1016/0092-8674(95)90401-8.
42. Lippman, S.M., Klein, E.A., Goodman, P.J., Lucia, M.S., Thompson, I.M., Ford, L.G., Parnes, H.L., Minasian, L.M., Gaziano, J.M., Hartline, J.A., et al. (2009). Effect of selenium and vitamin E on risk of prostate cancer and other cancers: the Selenium and Vitamin E Cancer Prevention Trial (SELECT). JAMA *301*, 39–51. https://doi.org/10.1001/jama.2008.864.
43. Rayman, M.P. (2012). Selenium and human health. Lancet *379*, 1256–1268. https://doi.org/10.1016/S0140-6736(11)61452-9.
44. Eagle, K., Jiang, Y., Shi, X., Li, M., Obholzer, N.D., Hu, T., Perez, M.W., Koren, J.V., Kitano, A., Yi, J.S., et al. (2022). An oncogenic enhancer encodes selective selenium dependency in AML. Cell Stem Cell *29*, 650. https://doi.org/10.1016/j.stem.2022.03.006.
45. Chiang, E.C., Shen, S., Kengeri, S.S., Xu, H., Combs, G.F., Morris, J.S., Bostwick, D.G., and Waters, D.J. (2009). Defining the Optimal Selenium Dose for Prostate Cancer Risk Reduction: Insights from the U-Shaped Relationship between Selenium Status, DNA Damage, and Apoptosis. Dose Response *8*, 285–300. https://doi.org/10.2203/dose-response.09-036.Chiang.
46. Esaki, N., Nakamura, T., Tanaka, H., and Soda, K. (1982). Selenocysteine lyase, a novel enzyme that specifically acts on selenocysteine. Mammalian distribution and purification and properties of pig liver enzyme. J. Biol. Chem. *257*, 4386–4391. https://doi.org/10.1016/S0021-9258(18)34734-3.
47. Ensor, C.M., and Tai, H.H. (1995). 15-Hydroxyprostaglandin dehydrogenase. J. Lipid Mediat. Cell Signal *12*, 313–319. https://doi.org/10.1016/0929-7855(95)00040-w.
48. Song, G., Zhao, R., and Zhao, W. (2008). Regulation of prostaglandin metabolism by selenium and its possible role in anticancer activity in LNCaP human prostate cancer cells. AACR.
49. Shirasaki, H., Kikuchi, M., Kanaizumi, E., and Himi, T. (2009). Accumulation of CRTH2-positive leukocytes in human allergic nasal mucosa. Ann. Allergy Asthma Immunol. *102*, 110–115. https://doi.org/10.1016/S1081-1206(10)60239-6.
50. Santus, P., and Radovanovic, D. (2016). Prostaglandin D2 receptor antagonists in early development as potential therapeutic options for asthma. Expert Opin. Investig. Drugs *25*, 1083–1092. https://doi.org/10.1080/13543784.2016.1212838.
51. Nagata, K., Tanaka, K., Ogawa, K., Kemmotsu, K., Imai, T., Yoshie, O., Abe, H., Tada, K., Nakamura, M., Sugamura, K., and Takano, S. (1999). Selective expression of a novel surface molecule by human Th2 cells in vivo. J. Immunol. *162*, 1278–1286. https://doi.org/10.4049/jimmunol.162.3.1278.
52. Cosmi, L., Annunziato, F., Galli, M.I.G., Maggi, R.M.E., Nagata, K., and Romagnani, S. (2000). CRTH2 is the most reliable marker for the detection of circulating human type 2 Th and type 2 T cytotoxic cells in health and disease. Eur. J. Immunol. *30*, 2972–2979. https://doi.org/10.1002/1521-4141(200010)30:10<2972::AID-IMMU2972>3.0.CO;2-#.

53. Bie, Q., Zhang, P., Su, Z., Zheng, D., Ying, X., Wu, Y., Yang, H., Chen, D., Wang, S., and Xu, H. (2014). Polarization of ILC2s in Peripheral Blood Might Contribute to Immunosuppressive Microenvironment in Patients with Gastric Cancer. J. Immunol. Res. *2014*, 923135. https://doi.org/10.1155/2014/923135.

54. Fukuoka, T., Yashiro, M., Morisaki, T., Kinoshita, H., Hasegawa, T., Kasashima, H., Masuda, G., Sakurai, K., Toyokawa, T., Tanaka, H., et al. (2014). The role of type D prostanoid receptors and PPARgamma in gastric cancer progression. Anticancer Res. *34*, 2771–2778.

55. Dash, P., Ghatak, S., Topi, G., Satapathy, S.R., Ek, F., Hellman, K., Olsson, R., Mehdawi, L.M., and Sjölander, A. (2022). High PGD(2) receptor 2 levels are associated with poor prognosis in colorectal cancer patients and induce VEGF expression in colon cancer cells and migration in a zebrafish xenograft model. Br. J. Cancer *126*, 586–597. https://doi.org/10.1038/s41416-021-01595-4.

56. Trabanelli, S., Chevalier, M.F., Martinez-Usatorre, A., Gomez-Cadena, A., Salomé, B., Lecciso, M., Salvestrini, V., Verdeil, G., Racle, J., Papayannidis, C., et al. (2017). Tumour-derived PGD2 and NKp30-B7H6 engagement drives an immunosuppressive ILC2-MDSC axis. Nat. Commun. *8*, 593. https://doi.org/10.1038/s41467-017-00678-2.

57. Wu, L., Lin, Q., Ma, Z., Chowdhury, F.A., Mazumder, M.H.H., and Du, W. (2020). Mesenchymal PGD(2) activates an ILC2-Treg axis to promote proliferation of normal and malignant HSPCs. Leukemia *34*, 3028–3041. https://doi.org/10.1038/s41375-020-0843-8.

58. Zhang, B., Bie, Q., Wu, P., Zhang, J., You, B., Shi, H., Qian, H., and Xu, W. (2018). PGD2/PTGDR2 Signaling Restricts the Self-Renewal and Tumorigenesis of Gastric Cancer. Stem Cell. *36*, 990–1003. https://doi.org/10.1002/stem.2821.

59. Crilly, S.E., and Puthenveedu, M.A. (2021). Compartmentalized GPCR Signaling from Intracellular Membranes. J. Membr. Biol. *254*, 259–271. https://doi.org/10.1007/s00232-020-00158-7.

60. Regad, T. (2015). Targeting RTK Signaling Pathways in Cancer. Cancers *7*, 1758–1784. https://doi.org/10.3390/cancers7030860.

61. Wong, K.K., Engelman, J.A., and Cantley, L.C. (2010). Targeting the PI3K signaling pathway in cancer. Curr. Opin. Genet. Dev. *20*, 87–90. https://doi.org/10.1016/j.gde.2009.11.002.

62. Fruman, D.A., and Rommel, C. (2014). PI3K and cancer: lessons, challenges and opportunities. Nat. Rev. Drug Discov. *13*, 140–156. https://doi.org/10.1038/nrd4204.

63. Burotto, M., Chiou, V.L., Lee, J.M., and Kohn, E.C. (2014). The MAPK pathway across different malignancies: a new perspective. Cancer *120*, 3446–3456. https://doi.org/10.1002/cncr.28864.

64. Nakanishi, H., Nakamura, T., Canaani, E., and Croce, C.M. (2007). ALL1 fusion proteins induce deregulation of EphA7 and ERK phosphorylation in human acute leukemias. Proc. Natl. Acad. Sci. USA *104*, 14442–14447. https://doi.org/10.1073/pnas.0703211104.

65. Pei, S., Minhajuddin, M., Callahan, K.P., Balys, M., Ashton, J.M., Neering, S.J., Lagadinou, E.D., Corbett, C., Ye, H., Liesveld, J.L., et al. (2013). Targeting aberrant glutathione metabolism to eradicate human acute myelogenous leukemia cells. J. Biol. Chem. *288*, 33542–33558. https://doi.org/10.1074/jbc.M113.511170.

66. Cai, X., Wang, C., Yu, W., Fan, W., Wang, S., Shen, N., Wu, P., Li, X., and Wang, F. (2016). Selenium Exposure and Cancer Risk: an Updated Meta-analysis and Meta-regression. Sci. Rep. *6*, 19213. https://doi.org/10.1038/srep19213.

67. Yenerall, P., Kollipara, R.K., Avila, K., Peyton, M., Eide, C.A., Bottomly, D., McWeeney, S.K., Liu, Y., Westover, K.D., Druker, B.J., et al. (2021). Lentiviral-Driven Discovery of Cancer Drug Resistance Mutations. Cancer Res. *81*, 4685–4695. https://doi.org/10.1158/0008-5472.CAN-21-1153.

68. Liu, Q., Chen, L., Atkinson, J.M., Claxton, D.F., and Wang, H.G. (2016). Atg5-dependent autophagy contributes to the development of acute myeloid leukemia in an MLL-AF9-driven mouse model. Cell Death Dis. *7*, e2361. https://doi.org/10.1038/cddis.2016.264.

69. Naviaux, R.K., Costanzi, E., Haas, M., and Verma, I.M. (1996). The pCL vector system: rapid production of helper-free, high-titer, recombinant retroviruses. J. Virol. *70*, 5701–5705. https://doi.org/10.1128/JVI.70.8.5701-5705.1996.

70. Barnes, K.M., Evenson, J.K., Raines, A.M., and Sunde, R.A. (2009). Transcript analysis of the selenoproteome indicates that dietary selenium requirements of rats based on selenium-regulated selenoprotein mRNA levels are uniformly less than those based on glutathione peroxidase activity. J. Nutr. *139*, 199–206. https://doi.org/10.3945/jn.108.098624.

71. Kasaikina, M.V., Kravtsova, M.A., Lee, B.C., Seravalli, J., Peterson, D.A., Walter, J., Legge, R., Benson, A.K., Hatfield, D.L., and Gladyshev, V.N. (2011). Dietary selenium affects host selenoproteome expression by influencing the gut microbiota. FASEB J *25*, 2492–2499. https://doi.org/10.1096/fj.11-181990.

72. Andrews, S. (2010). FastQC: a quality control tool for high throughput sequence data. Babraham Bioinformatics (Cambridge, United Kingdom: Babraham Institute).

73. Li, H., and Durbin, R. (2009). Fast and accurate short read alignment with Burrows-Wheeler transform. Bioinformatics *25*, 1754–1760. https://doi.org/10.1093/bioinformatics/btp324.

74. Li, H., Handsaker, B., Wysoker, A., Fennell, T., Ruan, J., Homer, N., Marth, G., Abecasis, G., and Durbin, R.; 1000 Genome Project Data Processing Subgroup (2009). The Sequence Alignment/Map format and SAMtools. Bioinformatics *25*, 2078–2079. https://doi.org/10.1093/bioinformatics/btp352.

75. Liao, Y., Smyth, G.K., and Shi, W. (2014). featureCounts: an efficient general purpose program for assigning sequence reads to genomic features. Bioinformatics *30*, 923–930. https://doi.org/10.1093/bioinformatics/btt656.

76. Ritchie, M.E., Phipson, B., Wu, D., Hu, Y., Law, C.W., Shi, W., and Smyth, G.K. (2015). limma powers differential expression analyses for RNA-sequencing and microarray studies. Nucleic Acids Res. *43*, e47. https://doi.org/10.1093/nar/gkv007.

77. Law, C.W., Chen, Y., Shi, W., and Smyth, G.K. (2014). voom: Precision weights unlock linear model analysis tools for RNA-seq read counts. Genome Biol. *15*, R29. https://doi.org/10.1186/gb-2014-15-2-r29.

CellPress
OPEN ACCESS

STAR★METHODS

KEY RESOURCES TABLE

REAGENT or RESOURCE	SOURCE	IDENTIFIER
Antibodies		
Annexin V (PE)	BioLegend	Cat# 640908; RRID: AB_2561298
Donkey anti-Goat IgG (H + L) Secondary Antibody, HRP	Invitrogen	Cat# A15999; RRID: AB_2534673
Goat anti-Mouse IgG (H + L) Secondary Antibody, HRP	Invitrogen	Cat# A16066; RRID: AB_2534739
Goat anti-Rabbit IgG (H + L) Secondary Antibody, HRP	Invitrogen	Cat# 31466; RRID: AB_10960844
goat polyclonal anti-TGFβ RIII (C-20)	Santa Cruz Biotechnology	Cat# sc-6199; RRID: AB_2303282
Mouse anti-human CD123 (6H6) (PE-Cyanine7)	eBioscience™	Cat# 25-1239-42; RRID: AB_1257136
Mouse anti-human CD34 (QBEND/10) (FITC)	eBioscience™	Cat# MA1-10204; RRID: AB_11154336
Mouse anti-human CD38 (HIT2) (APC)	eBioscience™	Cat# 17-0389-42; RRID: AB_1834353
Mouse anti-human CRTH-2 (APC)	R&D Systems	Cat# FAB3338A; RRID: AB_1964547
Mouse anti-human/mouse Phospho-4EBP1 (Thr36, Thr45) (V3NTY24) (eFluor 660)	eBioscience™	Cat# 50-9107-42; RRID: AB_2574319
Mouse anti-human/mouse Phospho-S6 (Ser235, Ser236) (cupk43k) (APC)	eBioscience™	Cat# 17-9007-42; RRID: AB_2573270
Mouse anti-mouse CD45.1 (FITC)	Miltenyi Biotec	Cat# 130-124-211; RRID: AB_2857674
Mouse monoclonal anti-EPHA7	Proteintech	Cat# 66667-1-Ig; RRID: AB_2882021
Mouse monoclonal anti-GAPDH (6C5)	Invitrogen	Cat# AM4300; RRID: AB_2536381
Mouse monoclonal anti-mTOR	BioLegend	Cat# 659201; RRID: AB_2563155
Mouse monoclonal anti-*p*-MEK-3/6 (B-9)	Santa Cruz Biotechnology	Cat# sc-8407; RRID: AB_627924
Mouse monoclonal anti-p53 (1C12)	Cell Signaling Technology	Cat# 2524; RRID: AB_331743
Mouse monoclonal anti-Raf-1 (E−10)	Santa Cruz Biotechnology	Cat# sc-7267; RRID: AB_628196
Mouse monoclonal anti-Vinculin	Proteintech	Cat# 66305-1-Ig; RRID: AB_2810300
Mouse monoclonal anti-β-Actin	Fitzgerald	Cat# 10R-2927; RRID: AB_11199124
Rabbit monoclonal anti-PTEN (138G6)	Cell Signaling Technology	Cat# 9559; RRID: AB_390810
Rabbit monoclonal anti-CREB (48H2)	Cell Signaling Technology	Cat# 9197; RRID: AB_331277
Rabbit monoclonal anti-4E-BP1 (53H11)	Cell Signaling Technology	Cat# 9644; RRID: AB_2097841
Rabbit monoclonal anti-p44/42 MAPK (Erk1/2) (137F5)	Cell Signaling Technology	Cat# 4695; RRID: AB_390779
Rabbit monoclonal anti-Phospho-Akt (Ser473) (D9E) XP®	Cell Signaling Technology	Cat# 4060; RRID: AB_2315049
Rabbit monoclonal anti-Phospho-*c*-Jun (Ser73) (D47G9) XP®	Cell Signaling Technology	Cat# 3270; RRID: AB_2129575
Rabbit monoclonal anti-Phospho-CREB (Ser133) (87G3)	Cell Signaling Technology	Cat# 9198; RRID AB_2561044
Rabbit monoclonal anti-Phospho-p44/42 MAPK (Erk1/2) (Thr202/Tyr204) (D13.14.4E) XP®	Cell Signaling Technology	Cat# 4370; RRID AB_2315112
Rabbit polyclonal anti-AKT	Cell Signaling Technology	Cat# 9272; RRID: AB_329827
Rabbit polyclonal anti-COX-1	Cayman Chemical Co.	Cat# 160109; RRID: AB_10077936
Rabbit polyclonal anti-CRTH2/DP_2 Receptor (N-Term)	Cayman Chemical Co.	Cat# 10004886; RRID N/A
Rabbit polyclonal anti-EGFR	ABclonal	Cat# A11351; RRID: AB_2861549
Rabbit polyclonal anti-FLT3	Proteintech	Cat# 21049-1-AP; RRID: AB_10733759

(*Continued on next page*)

Continued

REAGENT or RESOURCE	SOURCE	IDENTIFIER
Rabbit polyclonal anti-KRAS	Proteintech	Cat# 12063-1-AP; RRID: AB_878040
Rabbit polyclonal anti-MEK1/2	Cell Signaling Technology	Cat# 9122; RRID: AB_823567
Rabbit polyclonal anti-p70 S6 Kinase	R&D Systems	Cat# AF8962 RRID: AB_355696
Rabbit polyclonal anti-Phospho-4E-BP1 (Ser65)	Cell Signaling Technology	Cat# 9451; RRID: AB_330947
Rabbit polyclonal anti-Phospho-*c*-Raf (Ser259)	Cell Signaling Technology	Cat# 9421; RRID: AB_330759
Rabbit polyclonal anti-Phospho-mTOR (ser2481)	Cell Signaling Technology	Cat# 2974; RRID: AB_2262884
Rabbit polyclonal anti-Phospho-PI3 Kinase p85 (Tyr458)/p55 (Tyr199)	Cell Signaling Technology	Cat# 4228; RRID: AB_659940
Rabbit polyclonal anti-Phospho-PTEN (Thr382/383)	Proteintech	Cat# 29246-1-AP; RRID N/A
Rabbit polyclonal anti-PI 3-kinase p85α (Z-8)	Santa Cruz Biotechnology	Cat# sc-423; RRID: AB_632211
Rabbit polyclonal anti-Prostaglandin D Synthase (hematopoietic-type)	Cayman Chemical Co.	Cat# 160013; RRID: AB_327860
Rabbit polyclonal anti-TGFβ RII (H-567)	Santa Cruz Biotechnology	Cat# sc-1700; RRID:AB_632495
Rat anti-mouse CD117 (c-kit) (APC)	BioLegend	Cat # 105812; RRID: AB_313221
Rat anti-mouse CD117 (c-kit) (Alexa Fluor® 647)	BioLegend	Cat # 105818; RRID: AB_493474
Rat anti-mouse CD140b (PDGFRB) (PE)	eBioscience™	Cat# 12-1402-81; RRID: AB_529484
Rat anti-mouse Ly-6A/E (Sca-1) (PE-Cy™7)	BD Pharmingen™	Cat# 558162 RRID: AB_647253
Bacterial and virus strains		
One Shot™ Stbl3™ Chemically Competent E. coli	Thermo Fisher	Cat# C737303
Biological samples		
Human AML cells from peripheral blood	This study	N/A
Chemicals, peptides, and recombinant proteins		
Δ12-Prostaglandin J2	Cayman Chemical Co.	Cat# 18550
13,14-dihydro-15-keto Prostaglandin D2	Cayman Chemical Co.	Cat# 12610
15-deoxy-Δ12,14-Prostaglandin J2	Cayman Chemical Co.	Cat# 18570
15-deoxy-Δ12,14-PGJ2 ELISA kit	Enzo	Cat# ADI-900-023
2-Mercaptoethanol (BME)	Sigma Aldrich	Cat# M3148
[3H]-PGD2	Perkin Elmer	Cat# NET-616
Agarose LE	Denville scientific inc.	Cat# GR140-500
Akt Inhibitor	Calbiochem	Cat# 124005
Ammonium chloride	Sigma Aldrich	Cat# A-9434
Ampicillin	Sigma Aldrich	Cat# A0797
Annexin V Binding Buffer	BioLegend	Cat# 422201
ARS583	Cayman Chemical Co.	Cat# 19137
BAY293	Sigma Aldrich	Cat# SML2703
Betaplate scint	Perkin Elmer	Cat# 1205-440
BLUEstain™ Protein ladder, 11–245 kDa	Gibco	Cat# P007-500
Bovine Serum Albumin (BSA), Fraction V—Low-Endotoxin Grade	Gemini bio-products	Cat# 700-102P
BsmB I-v2 (200 unit)	New England Biolabs	Cat# R0739S
C-18 Sep-pak cartridge	Waters	Cat# WAT051910
CAY10471	Cayman Chemical Co.	Cat# 10006735
Cell Staining Buffer	BioLegend	Cat# 420201
Ciprofloxacin HCl	GoldBio.com	Cat# C-861-100
Citric acid monohydrate	Sigma	Cat# C-7129
CP-673451	MedChemExpress	Cat# HY-12050
CSF3 (G-CSF), Human	Gibco	Cat# 1120-02-10

(*Continued on next page*)

Continued

REAGENT or RESOURCE	SOURCE	IDENTIFIER
Dimethyl sulfoxide (DMSO)	Sigma Aldrich	Cat# D2438
Direct cAMP ELISA kit	Enzo	Cat# ADI-900-066
DMEM, high glucose, no glutamine	Gibco	Cat# 11960-044
Dulbecco's Modification of Eagle's Medium (DMEM)	Corning	Cat# 15-017-CM
Dulbecco's Phosphate-Buffered Saline	Corning	Cat# 21-031-CV
EDTA, Disodium Salt, Dihydrate, Molecular Biology Grade	Calbiochem	Cat# 324503
EGTA, Molecular Biology Grade	Calbiochem	Cat# 324626
Ethyl acetate	Fluka Analytical	Cat# 34972-2.5L-R
Fetal Bovine Serum - Premium (defined)	Atlanta Biologicals	Cat# S11150
Fetal Bovine Serum - Premium Select (undefined)	Atlanta Biologicals	Cat# S11550
Filtermat-B	Perkin Elmer	Cat# 1450-521
Fixation/Permeabilization concentration	eBioscience™	Cat# 00-5123-43
Fixation/Permeabilization Diluent	eBioscience™	Cat# 00-5223-56
G 418 Sulfate	Calbiochem	Cat# 345810
GentaMax® 100	Phoenix Pharm Distributors	Cat# 536086
GW9662	Cayman Chemical Co.	Cat# 70785
Hemavet	Drew Scientific Group	Hemavet 950FS
HEPES (1 M)	Gibco	Cat# 15630-080
Hexane, mixture of isomers	Sigma Aldrich	Cat# 650544-4L
Holo-transferrin, bovine	Sigma Aldrich	Cat# T1283
Holo-transferrin, human	Sigma Aldrich	Cat# T0665
HQL79	Cayman Chemical Co.	Cat# 10134
Human CRTH-2/GPR44 Overexpression Lysate	Novus Biologicals	Cat# NBL1-11281
Human FLT-3 Ligand	Shenandoah Biotechnology Inc.	Cat# 100-21
Human G-CSF	Shenandoah Biotechnology Inc.	Cat# 100-72
Human GM-CSF	Shenandoah Biotechnology Inc.	Cat# 100-08
human IL-3	Shenandoah Biotechnology Inc.	Cat# 100-80
Human SCF	Shenandoah Biotechnology Inc.	Cat# 100-04
Hydroxypropyl-b-cyclodextrin (HPBCD)	www.cyclodex.com	Cat# THPB-P
Imatinib (mesylate)	Cayman Chemical Co.	Cat# 13139
Insulin solution human	Sigma	Cat# I-9278
Iscove's Modified Dulbecco's Medium (IMDM)	Gibco	Cat# 12440-053
Koptec Pure Ethanol-200 Proof	Decon Labs, Inc.	DECON LABS #V1016
L-glutamine 200 mM (100×) solution	HyClone, Gelifesciences	Cat# SH30034.01
L-Selenomethionine	Sabinsa Corporation	Cat# G70452/H
LB Broth with agar (Miller)	Sigma Aldrich	Cat# L-3147
LY294002	Cayman Chemical Co.	Cat# 70920
M-PER mammalian protein extraction reagent, 250 mL	Thermo Fisher	Cat# 78501
Mammalian protein extraction reagent	Thermo Fisher	Cat# 78501
Magnesium chloride (MgCl2), anhydrous	Amresco	Cat# J364-500G
Methanol optima® LC/MS	Fisher Chemical	Cat# A456-4
Methocult M3234	Stem Cell Technologies	Cat# 032324
Mouse Interleukin-3 (IL-3)	Gemini bio-products	Cat# 300-324P
Mouse Interleukin-4 (IL-4)	Gemini bio-products	Cat# 300-325P

(*Continued on next page*)

Continued

REAGENT or RESOURCE	SOURCE	IDENTIFIER
Mouse Interleukin-6 (IL-6)	Gemini bio-products	Cat# 300-327P
Mouse Stem Cell Factor (SCF)	Gemini bio-products	Cat# 300-348P
Nitrocelllulose Blotting Membrane	GE Healthcare life science	Cat# 10600033
Paraformaldehyde, 16% w/v aq. soln., methanol free	Alfa Aesar	Cat# 43368
PD98059	Sigma Aldrich	Cat# 513000
Penicillin-Streptomycin Solution, 100×	Corning	Cat# 30-002-CI
PerfeCTa qPCR SuperMix	Quanta Bio	Cat# 95051-500
PerfeCTa SYBR Green SuperMix	Quanta Bio	Cat# 95055-500
Permeabilization buffer 10X	eBioscience™	Cat# 00-8333-56
Phenylmethylsulfonyl fluoride	Sigma Aldrich	Cat# P7626
Pierce™ BCA Protein Assay Reagent A	Thermo Fisher	Cat# 23228
Pierce™ BCA Protein Assay Reagent B	Thermo Fisher	Cat# 23224
Poly(ethyleneimine)	Supelco	Cat# P3143
Propidium iodide solution	BioLegend	Cat# 421301
Prostaglandin D2	Cayman Chemical Co.	Cat# 12010
Prostanoid CRTH2 (human) membrane preparation, in CHO-K1 cells	Perkin Elmer	Cat# ES-561-M400UA
Potassium Bicarbonate (KHCO3), Granular	JT. Baker	Cat# 2940-01
Protease Inhibitor Cocktail	Sigma Aldrich	Cat# P8340
Proteinase K	Greenbioresearchllc	Cat# GPR-10
Recombinant Mouse SCF (carrier-free)	BioLegend	Cat# 579702
Recombinant Murine Flt3-Ligand	Pepro Tech, INC.	Cat# 250-31L
Recombinant Murine IL-6	Pepro Tech, INC.	Cat# 216-16
RetroNectin® Recombinant Human Fibronectin Fragment	TaKaRa	Cat# T100A
RIPA buffer	Thermo Fisher	Cat# 89900
Rosiglitazone	Cayman Chemical Co.	Cat# 71740
Roswell Park Memorial Institute (RPMI) 1640	Corning	Cat# 10-040-CV
Sapanisertib (MLN0128)	Selleckchem	Cat# S2811
Saponin from quillaja bark	Sigma Aldrich	Cat# S7900
Selenium-adequate diet (0.08 ppm Se as selenite)	Harlan Teklad, Madison, WI	Cat# TD.07325
Selenium-deficient diet (<0.01 ppm Se as selenite)	Harlan Teklad, Madison, WI	Cat# TD.92163
Selenium-supplemented diet (0.4 ppm Se as selenite)	Harlan Teklad, Madison, WI	Cat# TD.07326
Sodium azide	Sigma Aldrich	Cat# S-2002
Sodium orthovanadate	Sigma Aldrich	Cat# S-6508
Sodium pyruvate (100mM) 100×	Gibco	Cat# 11360-070
Sodium selenite	Sigma Aldrich	Cat# S5261
StemSpanTM serum-free expansion medium II (SFEM II)	Stem Cell Technologies	Cat# 09655
Sucrose	Sigma Aldrich	Cat# S0389
SuperSignal™ West Pico PLUS Chemiluminescent Substrate	Thermo Fisher	Cat# 34580
T4 DNA ligase	New England Biolabs	Cat# M0202S
T4 Polynucleotide Kinase (500 units)	New England Biolabs	Cat# M0201S
Torin 1	Selleckchem	Cat# S2827
TransIT®-293 Reagent	MirusBio	Cat# MIR 2705

(*Continued on next page*)

Continued

REAGENT or RESOURCE	SOURCE	IDENTIFIER
TRI Reagent®	Sigma Aldrich	Cat# T9424
Trizma® hydrochloride	Sigma Aldrich	Cat# T3253
Trypan blue	VWR Life Science	Cat# VWRVK940
Trypsin-EDTA (0.25%), phenol red	Gibco	Cat# 25200-056
TWEEN® 20 BioXtra, viscous liquid	Sigma Aldrich	Cat# P7949
UltraPure™ DNase/RNase-Free Distilled Water	Invitrogen	Cat# 10977-015
Wortmannin	Sigma Aldrich	Cat# W1628
Critical commercial assays		
Bicinchoninic acid protein assay kit	Thermo Fisher	Cat# 23227
Cell counting kit-8 (CCK8)	Dojindo	Cat# CK04
EasySep mouse hematopoietic progenitor cell enrichment kit	Stem Cell Technologies	Cat# 19856A
High-capacity cDNA reverse transcription kit	Thermo Fisher	Cat# 4368813
MagniSortTM mouse CD45.1 positive selection kit	eBioscience™	Cat# 8802-6848-74
Plasmid Maxi Kit (25)	Qiagen	Cat#:12163
PureYield™ Plasmid Miniprep System	Promega	Cat# A1223
Wizard® SV Gel and PCR Clean-Up System (50 preps)	Promega	Cat# A9281
RNA 6000 Nano Kit	Agilent	Cat# 5067-1511
MGIEasy RNA Library Prep Kit	MGI Tech Co., Ltd	Cat# #1000006384
Deposited data		
RNAseq	GEO	GSE199629
Experimental models: Cell lines		
MOLM13	DSMZ	ACC-554
K562	ATCC	CCL-243™
HEK293T	ATCC	CRL-3467™
Phenix-Eco	ATCC	CRL-3214™
CHO K1	ATCC	CCL-61™
ES cell line Ptgdr2tm1(KOMP)Vlcg	Knockout Mouse Project Repository	MGI: 4843032
Experimental models: Organisms/strains		
C57/BL/6-Gpr44$^{-/-}$	Diwakar et al.[66]	N/A
Oligonucleotides		
sgRNA (1) for mouse *Kras*: Forward 5′-CACCCGGCTGAGGCGGCAGCGCTG-3′		N/A
sgRNA (1) for mouse *Kras*: Reverse 5′-AAACCAGCGCTGCCGCCTCAGCCG-3′		N/A
sgRNA (2) for mouse *Kras*: Forward 5′-CACCAGGCGGCAGCGCTGTGGCGG-3′		N/A
sgRNA (2) for mouse *Kras*: Reverse 5′-AAACCCGCCACAGCGCTGCCGCCT-3′		N/A
Recombinant DNA		
MSCV-human p210 BCR-ABL-IRES-GFP	Yenerall et al.[67]	Cat# 79248; RRID Addgene_79248
MSCV-MLL-AF9-EF1-luc2-p2A-EGFP-LC3	Liu et al.[68]	N/A
pCL-Eco	Naviaux et al.[69]	Cat# 12371; RRID Addgene_12371
pLV hU6-sgRNA hUbC-dCas9-KRAB-T2a-GFP	Thakore et al.[33]	Cat# 71237; RRID Addgene_71237

(*Continued on next page*)

Continued

REAGENT or RESOURCE	SOURCE	IDENTIFIER
pLV hU6-sgKRAS hUbC-dCas9-KRAB-T2a-GFP1	This study	Cat# 184556; RRID Addgene_184556
pLV hU6-sgKRAS hUbC-dCas9-KRAB-T2a-GFP2	This study	Cat# 184557; RRID Addgene_184557
pMD2.G	Didier Trono Lab (unpublished)	Cat# 12259; RRID Addgene_12259
psPAX2	Didier Trono Lab (unpublished)	Cat# 12260; RRID Addgene_12260
Software and algorithms		
7300 Real-time PCR system	Applied Biosystems	https://www.thermofisher.com/us/en/home/technical-resources/software-downloads/applied-biosystems-7300-real-time-pcr-system.html
AxioVision software	Zeiss	https://www.micro-shop.zeiss.com/en/us/system/software+axiovision-axiovision+program-axiovision+software/10221/
BD accuri C6 flow cytometer	BD Biosciences	https://www.bdbiosciences.com/en-us/products/instruments/flow-cytometers/research-cell-analyzers/bd-accuri-c6-plus
Cellometer K2 Fluorescent Cell Counter	Nexcelom Bioscience	https://www.nexcelom.com/nexcelom-products/cellometer-fluorescent-viability-cell-counters/cellometer-k2-fluorescent-viability-cell-counter/
FlowJo 10.8.0	BD	https://www.flowjo.com/solutions/flowjo/
Gene Set Enrichment Analysis	Broad institute	https://www.gsea-msigdb.org/gsea/index.jsp
GraphPad Prism version 6	GraphPad	https://www.graphpad.com/
IDEXX laboratories (Equine Health Panel)	IDEXX	https://www.idexx.com/en/
ImageJ	NIH	https://imagej.nih.gov/ij/
Ingenuity Pathway Analysis version 01-20-04	Qiagen	https://digitalinsights.qiagen.com/products-overview/discovery-insights-portfolio/analysis-and-visualization/qiagen-ipa/
MicroBeta2 Microplate Counters	Perkin Elmer	https://www.perkinelmer.com/product/microbeta2-plate-reader-with-2-detectors-2450-0020?utm_source=Google&utm_medium=cpc&utm_campaign=LSC-TEC-2022-AMER-PaidSearch-SCH-DG-ZZ&sfdc_id=7014V000002EAWQ&LS=PPC&adgroup=130890972930&ad=593625737509&keyword=microplate%20counter&gclid=Cj0KCQjw1ZeUBhDyARIsAOzAqQJ3in-8TXYWVxJ4u9T8__PmhQUi-6oReT-PwEZsjITxSWGbiCMYGMsaAjCJEALw_wcB
R software		Version 3.6.1
Other		
qPCR primers and probes	Table S4	

CellPress
OPEN ACCESS

RESOURCE AVAILABILITY

Lead contact

Further information and requests for resources and reagents should be directed to and will be fulfilled by the Lead Contact, K. Sandeep Prabhu (ksp4@psu.edu).

Materials availability

Plasmids generated in this study have been deposited with Addgene. Mouse lines and chemicals generated in this study will be made available to the broader scientific community upon request.

Data and code availability

- The raw FASTQ files and processed gene expression data of this study can be obtained from Gene Expression Omnibus (GEO) with an accession number of GSE199629.
- This paper does not report original code.
- Any additional information is available from the lead contact upon request.

EXPERIMENTAL MODEL AND SUBJECT PARTICIPANT DETAILS

Cell cultures

MOLM13 cells were maintained in Iscove's Modified Dulbecco's Medium (IMDM) supplemented with 20% (v/v) heat-inactivated fetal bovine serum (hi-FBS), 100 IU/mL Penicillin, and 100 μg/mL Streptomycin. K562 cells were maintained in Roswell Park Memorial Institute (RPMI) 1640 Medium supplemented with 10% (v/v) FBS, 100 IU/mL Penicillin, and 100 μg/mL Streptomycin. HEK293T and Phenix-Eco cells were maintained in DMEM containing 10% (v/v) FBS, 1 mM sodium pyruvate, 4 mM L-glutamine, 100 IU/mL of Penicillin, and 100 μg/mL of Streptomycin. Murine hematopoietic stem cells (HSCs) and leukemic cells isolated from spleens and bone marrows of transplanted mice were cultured in IMDM containing 15% (v/v) hi-FBS, 1% (w/v) bovine serum albumin (BSA), 10 μg/mL insulin, 20 μg/mL holo-transferrin, 2 mM L-glutamine, 0.007‰ (v/v) β-mercaptoethanol (BME), and 10 μg/mL ciprofloxacin supplemented with 25 ng/mL mouse recombinant (mr)- stem cell factor (SCF), 10 ng/mL mr-interleukin (IL)-3, 10 ng/mL mr-IL-6, and 25 ng/mL Flt3L. Primary patient AML cells were maintained in StemSpan Serum-Free Expansion Medium II (SFEM II) supplemented with 100 ng/mL human recombinant (hr)-SCF, 100 ng/mL hr-Flt3L, 20 ng/mL hr-IL-3, 20 ng/mL hr-G-CSF, 20 ng/mL hr-GM-CSF, 100 IU/mL Penicillin, and 100 μg/mL Streptomycin. Cells were cultured in a humidified 5% CO_2 incubator at 37°C.

Experimental animals

Male C57BL/6 mice were acquired from Taconic Biosciences. *Ai14*^{tdTomato} mice and CD45.1 mice were bred in house. All mice were provided *ad libitum* on specific diets based on their usages and maintained on MilliQ water to avoid the contamination of selenium from water. All animal studies were approved by the Institutional Animal Care and Use Committee (IACUC) at the Pennsylvania State University.

Generation of *Gpr44*$^{-/-}$ mice

Embryonic stem cells with C57BL/6 background lacking *Gpr44* gene were purchased from the Knockout Mouse Project Repository. In embryonic stem cells, *Gpr44* gene was deleted by inserting targeting vector into the translation start site of the third exon (Figure S4A). Female C57BL/6 mice with embryonic stem cell clones injected into blastocysts were maintained to generate chimeric mice. The male chimeric mice were bred with the female Cre transgenic mice to generate *Gpr44*$^{+/-}$*Cre*$^{+/-}$ mice. After several generations, *Gpr44*$^{-/-}$*Cre*$^{+/+}$ mice were stably maintained and confirmed by genotyping with primers: Reg-wtF + RegwtR and Reg-LacF + Reg-R (Figures S4A and S4B). To test the presence of GPR44 gene, tail-derived genomic DNA was used to perform PCR with primers for wild-type and for the targeted alleles.

Lentivirus cloning and production

psPAX2 (a gift from Didier Trono), pMD2.G (a gift from Didier Trono), pCL-Eco (a gift from Inder Verma),[69] and MSCV-human p210 BCR–ABL-IRES-GFP (a gift from Martine Roussel)[67] were obtained from Addgene. MSCV-MLL-AF9-EF1-luc2-p2A-EGFP-LC3 was received from Dr Gerard Grosveld (St. Jude Children's Research Hospital).[68] Retroviral stock for CML was generated by transfecting HEK293T cells with pCL-Eco and MSCV-human p210 BCR–ABL-IRES-GFP plasmids using TransIT 293 reagent (Figure S2A). Retroviral stock for AML was generated by transfecting Phenix-Eco cells with MSCV-MLL-AF9-EF1-luc2-p2A-EGFP-LC3 plasmid using TransIT 293 reagent (Figure S1A).

To knockdown the expression of KRAS, CRISPR/dCas9 system was adopted to target the promoter site of murine *Kras* gene. sgRNA target sequences were designed using CRISPick (https://portals.broadinstitute.org/gppx/crispick/public) with reference genome as "mouse GRCm38 (NCBI RefSeq v.108)" and enzyme as "SpyoCas9 (NGG)". Candidate oligomers for sgRNA were generated by adding respectively the overhang sequences "CACC" and "AAAC" to the 5′ end of forward and reverse oligos to facilitate the

cloning of oligomers into the BsmBI sites in the lentiviral transfer vector, pLV hU6-sgRNA hUbC-dCas9-KRAB-T2a-GFP (Addgene plasmid # 71237, a gift from Charles Gersbach).[33] Annealed DNA oligomers were prepared in the presence of T4 poly nuclease kinase at 37°C for 30 min. The lentiviral vector plasmid was cut with BsmBI-v2 (NEB) at 55°C for 1 h. In the presence of T4 DNA ligase, annealed DNA oligomers were inserted into the digested lentiviral transfer vector plasmid at the position of BsmBI following ligation at 4°C overnight. Transformation of the ligated plasmid was done on Stbl3 competent cells in an ampicillin LB-agar plate at 37°C overnight. Colonies were picked and growing overnight with shaking at 37°C in 5 mL of ampicillin LB culture. Plasmid DNA was prepared using the PureYield Plasmid Miniprep System (Promega) and Maxiprep System (QIAGEN) according to the manufacturer's protocol. Sanger sequencing was done using the plasmid DNA to verify the cloning and confirm the target site, BsmBI. To produce the lentivirus, verified plasmid, pLV hU6-sgRNA KRAS hUbC-dCas9-KRAB-T2a-GFP, was co-transfected with packaging plasmid, psPAX2 and envelope plasmid, pMD2.G into HEK293T cells using TransIT 293 reagent. Viral supernatants were harvested after 48 h and passed through a 0.45 μm filter. Viral stocks were stored at −80°C until further usage. Transfection efficiency was analyzed by monitoring the GFP expression in transfected HEK293T cells using fluorescent microscopy and flow cytometry.

Generation of experimental murine models of AML and CML

To generate WT AML murine model, CD45.1 WT female C57BL/6 mice and CD45.2 WT male C57BL/6 mice were used as donors and recipients, respectively. To generate Gpr44$^{-/-}$ AML murine model, CD45.2 Gpr44$^{-/-}$ female C57BL/6 mice and *Ai14*^{tdTomato} WT male mice were used as donors and recipients, respectively. To generate CML murine model, WT male mice were used as donors and recipients. Bone marrow cells in femurs and tibias of donor mice were flushed out using flow buffer (PBS with 2% FBS, 100 IU/mL Penicillin, and 100 μg/mL Streptomycin) and applied to red blood cell (RBC) lysis with ACK lysis buffer (155 mM NH_4Cl, 12 mM $KHCO_3$, 0.1mM EDTA-2Na). Then lineage-negative (Lin$^-$) cells were isolated using EasySep mouse hematopoietic progenitor cell isolation kit and stained with fluorescent antibodies Ly-6A/E (Sca-1) and Cd117 (c-Kit). HSCs were fluorescence-activated cell sorted (FACS) as Lin$^-$Sca-1$^+$c-Kit$^+$ population. Sorted HSCs were transduced with retrovirus in conditioned IMDM described above for 6 h. 1° transplantation was done by retro-orbital injection of retrovirus-transduced HSCs into sub-lethally irradiated (4.75 Gy) recipients. For CML, 1° recipient mice were used for experiments and received treatments when the peripheral WBCs reached 5 K/μL. For AML, 1° recipient mice were euthanized when they showed symptoms of full-blown leukemia; and leukemic splenocytes were isolated by meshing spleen with flow buffer followed by RBC lysis and transplanted into non-irradiated 2° recipients. Water containing antibiotics (GentaMax 100) was supplied to prevent opportunistic digestive infections from three days prior to transplantation to seven days post transplantation if irradiation was applied.

METHOD DETAILS

Serial transplantation and survival analyses

2° transplantation of AML was performed retro-orbitally by transplanting 4 × 10^5 leukemic splenocytes per mouse from primarily transplanted mice into 2° recipients. Competitive transplantation was done with AML donor cells as follows: WT (4 × 10^5 per mouse), WT plus Gpr44$^{-/-}$ (2 × 10^5 + 2 × 10^5 per mouse), and Gpr44$^{-/-}$ (4 × 10^5 per mouse). 3° transplantation was done retro-orbitally by transplanting 4 × 10^5 leukemic splenocytes per mouse from secondarily transplanted mice into 3° recipients. For survival analysis with dietary intervention, recipient mice were maintained on Se-A or Se-S diet and water *ad libitum* for four weeks prior to transplantation and sustained on the same diets until the endpoints. For other survival analyses, all the recipient mice were administered normal chow diet and water *ad libitum*. The endpoint events include: 1) death, 2) WBCs in the periphery >50 K/μL, 3) paralysis, 4) immobility, and 5) hypothermia. The observation period was two months post transplantation or ceased when event(s) occurred before the end of the period.

Purification of AML cells

To purify WT and Gpr44$^{-/-}$ AML cells, MagniSort mouse CD45.1 positive selection kit was used. Briefly, CD45.2 recipient mice transplanted with CD45.1 WT AML donor cells or CD45.1 recipient mice transplanted with CD45.2 Gpr44$^{-/-}$ AML donor cells were euthanized at the endpoint. Splenocytes were isolated and applied to RBC lysis. Donor and recipient mixed splenocytes were resuspended in flow buffer. Anti-Mouse CD45.1 Biotin was added into the suspension and incubated at room temperature for 10 min. Positive Selection Beads A were added to bind CD45.1 antibody and CD45.1$^+$ cells were kept in the magnets while CD45.1$^-$ cells were eluted. Purified WT AML cells and Gpr44$^{-/-}$ AML cells were harvested as CD45.1$^+$ and CD45.1$^-$ populations, respectively.

Dietary treatments

To examine the effect of Se supplementation at supraphysiological levels on the outcome of AML. 2° recipient mice were maintained on special diets varying in Se for four weeks prior to transplantation and continued on the same diets until the endpoints of experiments. Details are described in figure legends. Se-D (containing less than 0.01 ppm background Se), Se-A (0.08 ppm Na_2SeO_3), and Se-S (0.4 ppm Na_2SeO_3) diets were commercially purchased from Harlan Teklan, Madison, WI, USA. To compare inorganic and organic Se-S diets at different doses, commercial Se-D diet was used as a base to formulate 0.4 ppm and 1.0 ppm Na_2SeO_3 and 0.8 ppm and 3.0 ppm SeMet. Briefly, Se-D diet was pestled to powder. And 0.4 mg and 1.0 mg Na_2SeO_3 were added

into the powder of 1 kg to formulate custom 0.4 ppm and 1.0 ppm Na_2SeO_3 diets, respectively. Similarly, 0.8 mg and 3.0 mg SeMet were added into the powder of 1 kg to formulate custom 0.8 ppm and 3.0 ppm SeMet diets, respectively. Solid strip-shape diets were manually molded. Dietary levels of Se used in this study were selected based on previous literature.[15,70,71]

In-vivo inhibition of H-PGDS

in vivo treatment of HQL79 (10 mg/kg body weight; daily) was utilized to inhibit the activity of H-PGDS. Experimental mice were kept on Se-S diet for four weeks prior to 2° transplantation with CD45.1 WT AML donor cells and maintained until euthanasia. At one week post transplantation, mice were injected intraperitoneally with HQL79 for two weeks. HQL79 stock was suspended in citric acid and prepared in 25 mM (2-Hydroxypropyl)-β-cyclodextrin (HPBCD) for injection.

In-vivo treatment of CyPGs

Mice on Se-A diet were treated with CyPGs as follows. Experimental mice were kept on diet for four weeks before transplantation. For AML, treatment of four CyPG compounds (DK-PGD_2, 15d-PGJ_2, Δ^{12}-PGJ_2, and Δ^{12}-PGJ_3; 0.2 mg/kg body weight; daily) was administered intraperitoneally at one week post transplantation for two weeks to the 2° recipient mice transplanted with 1° CD45.1 WT AML donor cells. For CML, treatment of DK-PGD_2 (0.2 mg/kg body weight; daily) was administered intraperitoneally starting at the point when blood WBCs reached 5 K/μL after transplantation for two weeks to the 1° recipient mice transplanted with WT CML HSCs. CyPG stocks were suspended in organic solvent (methyl acetate or ethyl acetate). All four compounds were freshly dried under gas nitrogen and resuspended in PBS before intraperitoneal injection.

In-vivo modulation of PPARγ

Mice on Se-S diet were treated with PPARγ modulators as follows. Mice were kept on Se-S diet for four weeks before 2° transplantation with 1° $Gpr44^{-/-}$ AML donor cells until euthanasia. Treatment of PPARγ antagonist GW9662 (1 mg/kg body weight) was administered intraperitoneally every other day for two weeks at one week post transplantation. Treatment of PPARγ agonist rosiglitazone (6 mg/kg body weight) was administered intraperitoneally daily for two weeks at one week post transplantation. GW9662 and rosiglitazone stocks were dissolved in dimethyl sulfoxide (DMSO) and prepared in PBS for injection.

In-vitro treatment of Na_2SeO_3

MOLM13 cells were seeded in 96-well plates at a density of 4×10^3 cells per well in the presence of 1 μM Na_2SeO_3 for 0, 24, 48, 72, and 96 h. 10 μL of CCK8 solution was added to the plates. After 4 h incubation at 37°C, the plates were measured for absorbance at 450 nm using a microplate reader.

In-vitro treatment of CyPGs

MOLM13 cells were seeded in 96-well plates at a density of 5×10^3 cells per well. Four CyPG compounds (DK-PGD_2, 15d-PGJ_2, Δ^{12}-PGJ_2, and Δ^{12}-PGJ_3) were added to the plates with serial diluted concentrations of 0, 10, 100, 500, 1,000, 2,500, and 5,000 nM. After 96 h culture, 10 μL of CCK8 solution was added to the plates. After 4 h incubation at 37°C, the plates were measured for absorbance at 450 nm using a microplate reader. To analyze time-dependent effect of Δ^{12}-PGJ_3, 5×10^3 MOLM13 cells/well in a 96-well plate were cultured in the presence of 500 nM Δ^{12}-PGJ_3 for 0, 24, 48, 72, and 96 h. Cell viability was measured using CCK8 solution as described above.

K562 cells were seeded in 96-well plates at a density of 4×10^4 cells per well. DK-PGD_2 was used to treat the cells with serially diluted concentrations of 0, 0.5, 1.0, and 2.5 μM. After 24, 48, and 72 h culture, viability of cells was measured using CCK8 kit as described above.

$CD45.1^+Lin^-$ $Sca\text{-}1^-c\text{-}Kit^+$ FACS-sorted WT AML LICs were generated from bone marrow and spleen of secondarily transplanted AML recipient mice. 5×10^3 cells per well were seeded in 96-well plates and cultured in the presence of CyPGs (DK-PGD_2, 15d-PGJ_2, Δ^{12}-PGJ_2, and Δ^{12}-PGJ_3) with the final concentration of 500 nM for four days. CyPGs were prepared in 5 μL PBS and added daily to each well accordingly. Cell viability was measured using CCK8 solution as described above.

Lin^- WT AML splenocytes from primarily transplanted AML recipient mice were plated in 12-well plates at a density of 5×10^6 cells per well. CyPGs (DK-PGD_2, 15d-PGJ_2, Δ^{12}-PGJ_2, and Δ^{12}-PGJ_3) were applied to cells at a concentration of 25 nM for 24 h. Cells were harvested for western immunoblotting.

Primary AML cells isolated from peripheral blood of AML patients with written informed consent were from the tissue bank at the Penn State Cancer Institute. Clinical characteristics of patient AML cells are listed in Table S2. DK-PGD_2 and 15d-PGJ_2 were used to treat the cells with the final concentration of 500 nM for three days. Δ^{12}-PGJ_3 was used to treat patient AML cells at a concentration of 100 nM for 6 h in the presence or absence of 10 nM CAY10471. At the endpoint, cells were harvested, stained with fluorescent antibodies, and measured under a BD Accuri C6 flow cytometer. This experiment was approved by the Institutional Review Board and Institutional Biosafety Committee at Penn State University.

In-vitro inhibition of KRAS

2° Gpr44$^{-/-}$ AML splenocytes were seeded in 96-well plates at a density of 1 × 10^4 cells per well. BAY293 stock was stored in DMSO and prepared to treat the cells at the concentrations of 0, 0.25, 0.5, 1.0, 2.0, and 4.0 μM for 48 h. BAY293 with high concentrations of 0, 5, 10, and 15 μM were applied to cells for 24 and 48 h. Cell viability was measured using CCK8 solution.

Purified 2° CD45.2 Gpr44$^{-/-}$ AML cells were seeded in a 6-well plate at a density of 4 × 10^6 cells per well. After culturing in the absence or presence of 15 μM BAY293 for 48 h, cells were harvested and stained with acridine orange and propidium iodide (AO/PI) staining solution. Live/dead cell counts were acquired by a cellometer (Nexcelom Bioscience).

In-vitro knockdown of KRAS via CRISPRi

Knockdown of KRAS expression was done on both purified 1° and 2° CD45.2 Gpr44$^{-/-}$ AML cells. Briefly, purified 1° Gpr44$^{-/-}$ AML cells were cultured in the presence of pLV hU6-sgRNA KRAS hUbC-dCas9-KRAB-T2a-GFP viral supernatants for 24 h while purified 2° Gpr44$^{-/-}$ AML cells were cultured in the same viral supernatants for 30 h prior to 3° transplantation. Knockdown of KRAS was verified by western immunoblotting.

In-vitro inhibition of ERK

2° Gpr44$^{-/-}$ AML splenocytes were seeded in 6-well plates at a density of 5 × 10^6 cells per well. PD98059 was dissolved in DMSO and used to treat the cells with the final concentration of 0, 10, 50, and 100 μM for 0, 24, 48, and 72 h. For 3° transplantation, 100 μM PD98059 was applied to 2° Gpr44$^{-/-}$ AML splenocytes for 24 h prior to transplantation.

In-vitro inhibition of PI3K, AKT, and MTORC

Purified 1° Gpr44$^{-/-}$ AML splenocytes were seeded in 96-well plates at a density of 1 × 10^4 cells per well. LY294002, Wortmannin, Sapanisertib, and Torin 1 stocks were stored in DMSO and prepared to treat the cells for 24 h at the concentration of 10 μM, 10 nM, 10 nM, and 250 nM, respectively. Cell viability was measured using CCK8 solution.

In-vitro inhibition of RTKs and PDGFR

Purified 2° Gpr44$^{-/-}$ AML splenocytes were seeded in 96-well plates at a density of 1 × 10^4 cells per well. Imatinib were stored in DMSO and prepared to treat the cells at the concentration of 0, 0.1, 1, 10, and 100 μM for 18 h. CP-673451 were stored in DMSO and prepared to treat the cells at the concentration of 0, 1, 10, 100, and 1,000 nM for 18 h. Cell viability was measured using CCK8 solution.

Methylcellulose culture

Leukemic cells were cultured in methylcellulose medium supplemented with 25 ng/mL mr-SCF, 10 ng/mL mr-IL-3, and 10 ng/mL mr-IL-6. Cells were cultured in at least triplicate in a 5% CO_2 incubator at 37°C. Detailed treatments were described in each figure legends accordingly. Colonies were counted at least after one week incubation and classified under the microscope. Images were obtained under a microscope installed with AxioVision software.

Measurement of 15d-PGJ$_2$ by enzyme-linked immunoassay (ELISA)

Whole blood samples were collected by performing cardiac puncture at endpoint. Sera were isolated by centrifugation for 15 min at 8,000 rpm at 4°C and used to measure 15d-PGJ$_2$ with a specific ELISA kit (Enzo Life Sciences) as described earlier.[16]

Measurement of cyclic adenosine monophosphate (cAMP) by ELISA

2° WT and Gpr44$^{-/-}$ AML cells were purified using MagniSort mouse CD45.1 positive selection kit as described above. 1 × 10^6 cells were suspended in PBS with 0, 0.5, and 1.0 μM DK-PGD$_2$ for 30 min in a 5% CO_2 incubator at 37°C. Cell pellets were harvested by centrifugation for 3 min at 600 *g* at 4°C. 0.1 M HCl of 0.5 mL was used to lyze the cell pellets for 20 min at room temperature. Cellular debris were removed by centrifugation for 3 min at 600 *g*. The supernatants were stored at −80°C until further analysis. 0.1 mL supernatants were assayed in the acetylated format for the measurement of cAMP using a competitive ELISA kit (Enzo Life Sciences) according to the manufacturer's instruction.

Measurement of apoptosis

Patient AML cells isolated from peripheral blood were resuspended in cell staining buffer and then stained by CD34 (1:100), CD38 (1:100), and CD123 (1:100) fluorescent antibodies for 30 min at room temperature. Cells were washed twice by cell staining buffer and resuspended in Annexin V binding buffer and incubated at room temperature for 15 min in the presence of PE Annexin V antibody followed by flow cytometric analysis.

Measurement of cell cycle

5 × 10^6 1° CD45.1 WT and Gpr44$^{-/-}$ AML cells were washed in 1 mL sterile PBS by centrifugation for 3 min at 850 *g* at 4°C. Cell pellets were fixed in 70% (v/v) ethanol for 30 min at 4°C and then washed twice with PBS by centrifugation for 3 min at 850 *g* at 4°C. Cells were suspended in 250 μL PBS containing 20 μg/mL ribonuclease, 20 μL PI, and 1 μL FITC-CD45.1 antibody and incubated

on ice at dark for 20 min. Raw data were collected on BD Accuri C6 and analyzed using FlowJo version 10. Cells were first gated on FSC-A/FSC-H and FSC-A and SSC-A to acquire singlets. AML cells were identified as CD45.1$^+$ population and further evaluated for cell cycle phase using Dean-Jet-Fox Model in FlowJo.

FACS analysis

Nucleated cells in blood, bone marrow, and whole spleen were collected from mice at endpoint. Peripheral blood collected from 1° CML mice was applied to RBC lysis and single cell suspensions were used to detect GFP frequency under BD Accuri C6. Bone marrow cells were flushed out from femurs and tibias using flow buffer followed by RBC lysis. Whole spleen cells were isolated by meshing spleen with flow buffer in 70 μm cell strainers followed by RBC lysis. Single cell suspensions were applied to perform hematopoietic progenitor cell isolation according to the manufacturer's instruction, and then stained with Cd117 (c-Kit) and Ly-6A/E (Sca-1) fluorescent antibodies. Raw data of Lin$^-$ cell numbers and the presence of LICs were collected on BD Accuri C6 and analyzed using FlowJo version 10. WT and Gpr44$^{-/-}$ AML LICs were identified as CD45.1$^+$Lin$^-$Sca-1$^-$c-Kit$^+$ (Figure S1I) and RFP$^-$Lin$^-$Sca-1$^-$c-Kit$^+$ (Figure S4E) populations, respectively. Normal recipient HSCs were recognized as CD45.1$^-$Lin$^-$ Sca-1$^+$c-Kit$^+$ population. WT CML LICs were identified as GFP$^+$Lin$^-$Sca-1$^+$c-Kit$^+$ population (Figure S2D).

For intracellular staining assay, 1° Gpr44$^{-/-}$ AML cells were washed twice with PBS and incubated with CD45.1 antibody in flow buffer for 30 min at room temperature. Then cells were fixed using 4% paraformaldehyde for 40 min, permeabilized for 50 min and stained separately with primary antibodies (Phospho-4E-BP1 and Phospho-S6K; 1:100) in permeabilization buffer for 30 min at room temperature. MOLM13 cells were washed twice with PBS and resuspended in 2% paraformaldehyde. After 10 min incubation at room temperature, cells were washed with PBS and resuspended in permeabilization buffer [3% FBS (v/v), 0.1% saponin (w/v), 0.09% sodium azide (w/v)]. GPR44 antibody (1:100) was added into the cell suspension with 30 min incubation at 4°C. Raw data were collected on BD Accuri C6 and analyzed using FlowJo version 10.

Western immunoblotting

Total proteins were extracted from different cells from various experiments using M-PER (Mammalian Protein Extraction Reagent) from Thermo Fisher Scientific containing protease inhibitor complex and 5 mM sodium orthovanadate (Sigma). Cell lysates were incubated on ice for 30 min and then centrifuged for 10 min at 12,000 *g*, 4°C. Supernatants were quantified using a Bicinchoninic Acid Protein Assay Kit (Thermo Fisher Scientific) for protein concentration.

Membrane proteins were extracted from MOLM13 cells using (pH 7.4) 20 mM HEPES buffer with 2 mM EDTA and protease inhibitor complex. Cell lysates were homogenized and spined down at 1,000 *g*, 4°C for 5 min. Pellets were resuspended in (pH 7.4) 20 mM HEPES with 2 mM EDTA and protease inhibitor complex and applied to homogenesis and centrifugation again. Remaining pellets were resuspended in 5 mL HEPES buffer and applied to centrifugation at 100,000 *g*, 4°C for 1 h twice. Cell pellets were dissolved in RIPA buffer. Protein concentration was measures in the same way described above.

15∼30 μg Proteins were loaded onto SDS-PAGE gels and then transferred onto nitrocellulose blotting membranes. Blots were blocked in 5% milk and incubated with primary antibodies over night at 4°C; secondary antibodies were goat anti-rabbit (Thermo Fisher Scientific) and goat anti-mouse (Thermo Fisher Scientific). Blots developed with West Pico reagent (Thermo Fisher Scientific) were scanned in an imaging system (G:Box Chemi) with GeneSys software program (Version 1.5.7.0). Experiments were performed in at least triplicate. Densitometry analysis was done by ImageJ software (National Institutes of Health, Bethesda, MD).

qPCR

Total RNAs were extracted from cells in TRI reagent (Sigma) according to manufacturer's instructions. RNA concentrations were measured by Nanodrop One (Thermo Scientific). 0.5–1.0 μg RNAs were used to synthesize cDNA by a High-Capacity cDNA Reverse Transcription Kit (Thermo Fisher Scientific). cDNA was applied to perform qPCR using PerfeCTa qPCR SuperMix or PerfeCTa SYBR Green SuperMix (Quanta Biosciences) in a 7300 Real-time PCR system (Applied Biosystems). TaqMan probes and primers were listed in "key resources table". Data were analyzed using the method of Livak and Schmittgen and normalized to *18S* ribosomal RNA (rRNA), *Gapdh*, or *Bactin*.

RNAseq analysis

Sample preparation

WT and Gpr44$^{-/-}$ AML LICs were used for RNA sequencing. At the endpoint, femurs and tibias were sampled from 2° CD45.2 or *Ai*^{14TdTomato} recipients of full-blown AML transplanted with CD45.1 WT or Gpr44$^{-/-}$ AML donor cells, respectively. Lin$^-$ cells were isolated using EasySep mouse hematopoietic progenitor cell isolation kit and stained with fluorescent antibodies Ly-6A/E (Sca-1) and Cd117 (c-Kit) as well as CD45.1 antibody for WT AML. 4×10^5 WT and Gpr44$^{-/-}$ AML LICs were sorted under a Beckman Coulter MoFlo Astrios EQ Cell Sorter as CD45.1$^+$Sca-1$^-$c-Kit$^+$ or RFP$^-$Sca-1$^-$c-Kit$^+$ populations, respectively. Meanwhile, bone marrow Lin$^-$Sca-1$^-$c-Kit$^+$ cells were also sorted from normal mice.

RNA-Seq library preparation, sequencing, and alignment

Total RNA was extracted using TRI reagent and the measurement of RNA quality with RNA Integrity Number (RIN) and *28S*/*18S* was done by an RNA 6000 Nano kit on an Agilent 2100 Bioanalyzer system. Library preparation for next generation sequencing was performed by using MGIEasy RNA Library Prep Kit according to the manufacturer's instructions. RNA sequencing was performed

for each sample by using DNA nanoball sequencing technology on a DNBSEQ-T7 sequencer with 40 million 100 bp paired-end reads. Sequence quality per based was checked by FastQC (v0.11.2).[72] The filtered reads were aligned to the GRCm38.p6 (mm10) from EMBL-EBI with Burrows-Wheeler Aligner (BWA, v 0.7.17-r1188).[73] The large nucleotide sequence alignments were sorted and indexed, and the alignment reports were generated by using SAMtools (v1.10).[74] The raw count matrix for genes was obtained from featureCounts (v2.0.0).[75] Genes were annotated against the GENCODE vM18 from EMBL-EBI while generating the count matrix.

Differential gene expression analysis

The differential gene expression analysis was conducted by using the limma package in R software.[76] Genes with a count per million (CPM) more than 0.5 in at least two samples were kept. Voom transformation was applied for implementing the normalization factors which estimating the mean-variance relation to determine the sample weight.[77] The Empirical Bayes Rule was also implemented to shrink the variance. The t statistics and the p-values were estimated under two sample t tests using the eBays function within the limma package in R software. The false discovery rate (FDR) was obtained from the multiple testing corrections for the type I errors under the Benjamini-Hochberg (BH) Procedure. Principal component analysis (PCA) and hierarchical clustering analysis were performed based on the top 500 variable genes to elucidate the relationship between samples. Heatmap was plotted to show the gene variations across samples by using the heatmap.2 function in gplots package. Volcano plots were generated by using the ggplots package.

Gene set enrichment analysis (GSEA)

Enriched pathways were determined by using the GSEA tool available from the Broad Institute website. Significantly enriched gene sets with adjusted *p* values (Benjamini-Hochberg procedure) between two groups was detected by differential gene expression analysis. GSEA plots were done using the GSEA program (version 4.1.0). The signature collections from the Molecular Signatures Database (MSigDB) (http://software.broadinstitute.org/gsea/msigdb) were listed in Table S3 with normalized enrichment score (NES), *p* value, and Q value.

Ingenuity pathway analysis (IPA)

Comparison datasets, *i.e.*, 1) WT AML LICs versus normal Lin^{-}Sca-1^{-}c-Kit^{+} cells and 2) Gpr44$^{-/-}$ AML LICs versus WT AML LICs, generated from differential gene expression analysis were uploaded to QIAGEN IPA application (Version 01-20-04). Core and comparison analyses were conducted according to the manufacturer's instructions. Canonical pathways were analyzed in core analysis in each datasets by setting the cutoffs: LogFC (Expr Log Ratio) −1.4 to 1.4 and p value <0.05. Comparison analysis was performed by comparing the above core analysis results to identify the effect of GPR44 deletion in the background of AML.

ONCOMINE analysis

Comparisons of gene expression between healthy people and leukemia patients and within the FAB subtype groups was performed by extracting data from ONCOMINE Platform (https://www.oncomine.org/), including GPR44, PPARG, and NFKB genes [NFκB-1, NFκB-2, NFκB-3/RelA, RelB, c-Rel, NF-κB Inhibitor Alpha (NFκBIA)]. The available information includes: statistics (the name of the cohort), comparison (the disease type), p-values, t-tests, fold change, gene rank, number of measured genes, gene type (mRNA or DNA), total sample size, specific sample size, details (sequencing procedure), reporter (data organizer), and publication Information with date. Since the ONCOMINE organizes the results in over-expression model and under-expression model separately with single sided t test, we determined the over- or under-expression of a gene in one study based on its reported fold change and then extracted the corresponding p-value and gene rank to determine its significance. Volcano plots were generated to visualize and compare the gene expressions by using ggplot2 packages in R software (Version 3.6.1).

Hematology

20–25 μL Peripheral blood was collected retro-orbitally, and then complete blood cell counts including white blood cell (WBC), neutrophil (NE), lymphocyte (LY), monocyte (MO), eosinophil (EO), and basophil (BA) were analyzed on a hemavet 950FS. Leukocytosis was also monitored by evaluating the peripheral blood in primarily transplanted mice.

Biochemistry analysis

Heart puncture was done on mice secondarily transplanted with either WT or Gpr44$^{-/-}$ AML donor cells to acquire whole blood samples. Sera were isolated by centrifugation for 15 min at 8,000 rpm at 4°C and biomarkers of renal and liver function were analyzed using a panel test from IDEXX Laboratories (https://www.idexx.com/en/).

Histological analysis

Murine spleens and livers were isolated at the endpoint and fixed in 10% (v/v) buffered formalin. The fixed tissues were embedded by paraffin and cut into sections. Subsequently, sections were stained with hematoxylin and eosin (H&E). Images were obtained under a microscope installed with AxioVision software for histological analysis.

CellPress
OPEN ACCESS

Radioligand binding assay

For human prostanoid CRTH2 receptor (PerkinElmer # ES-561-M400UA) binding, 5 μg membrane proteins were incubated with 3H-labeled PGD_2 [5,6,8,9,12,14,15-3H(N)] (10 nM) in the presence or absence of increasing concentrations (from 10 pM to 10 μM) of either PGD_2, or Δ^{12}-PGJ_2 or Δ^{12}-PGJ_3 (E-isomer) for competition binding. The binding reactions were carried out for 60 min at 27°C in a final volume of 0.2 mL of 50 mM Tris-HCl (pH 7.4) containing 5 mM $MgCl_2$. Cold PGD_2 (50 μM) was used to define non-specific binding. All binding reactions were terminated by filtration under vacuum onto polyethyleneimine (0.3%) presoaked Filtermat-B followed by 6 brief washes with 4 mL of ice-cold TE buffer. Membranes were dried overnight on a heating block at 37°C. Bound radiolabel was determined by liquid scintillation counting using MicroBeta[2] Microplate Counter.

QUANTIFICATION AND STATISTICAL ANALYSIS

All experiment statistical analyses were analyzed using GraphPad Prism version 6 (GraphPad Software) and presented as the mean ± SEM. For the comparison between two groups, unpaired one-tailed Student t test was utilized. For the comparison between (more than two) groups, two-way *ANOVA* followed by appropriate *post hoc* tests (Bonferroni correction) was applied. Variation from these analyses and replicate numbers are described in figure legends. Survival analysis was performed using the Log rank (Mantel-Cox) test. p value <0.05 was considered significant, *, $p < 0.05$; **, $p < 0.01$.